The Impact of Radiative Heat Transfer in Combustion Processes and Its Modeling – with a Focus on Turbulent Flames

Fengshan LIU[1], Jean-Louis CONSALVI[2,†], Pedro J. COELHO[3], Frédéric ANDRE[4], Mingyan GU[5, †], Vladimir SOLOVJOV[6], Brent W. WEBB[6]

[1] Metrology Research Centre, National Research Council of Canada, 1200 Montreal Road, Ottawa, Ontario K1A 0R6, Canada
[2] Aix-Marseille Université, IUSTI/ UMR CNRS 7343, 5 rue E. Fermi, 13453 Marseille, France
[3] Mechanical Engineering Department, IDMEC, Instituto Superior Técnico, Universidade de Lisboa, Lisbon, Portugal
[4] Univ Lyon, CNRS, INSA-Lyon, Université Claude Bernard Lyon 1, CETHIL UMR5008, F-69621 Villeurbanne, France
[5] School of Energy and Environment, Anhui University of Technology, Ma'anshan, China 243002
[6] Brigham Young University, 360G EB, Provo, UT 84602, USA

[†] Corresponding author: Tel.: +33-491-106-831; Fax: +33-491-106-969.
E-mail address: jean-louis.consalvi@univ-amu.fr; gumy@ahut.edu.cn

Abstract
Radiative heat transfer (RHT) is often the dominant mode of heat transfer in flames, fires, and combustion systems and affects significantly temperature distributions directly and kinetically controlled chemical processes indirectly. Modeling RHT accurately in multidimensional flames and combustion systems is challenging mainly due to the highly spectral dependence of radiative properties of combustion products, the high computational cost of solving the radiative transfer equation (RTE), and the strong turbulence and radiation interactions (TRI). Significant progress has been made in all the three aspects in the last three decades and the state-of-the-art models and methods have been incorporated into CFD practice for modeling fires, turbulent jet flames, and turbulent combustion in combustion systems. In this article, we first discuss the coupling between RHT and combustion and the important role played by RHT in some fundamental flame phenomena. Then we discuss the state-of-the-art radiation models with a focus on RTE solvers, radiative property models and TRI. Next, we review the recent simulations of turbulent combustion systems involving these state-of-the-art radiation models. Finally, we provide concluding remarks and some potential research areas to advance RHT modeling in multiphase reacting flows.

Nomenclature

A_x, A_y, A_z area normal to directions x, y and z [m^2]
a non-grey stretching factor for WSGG, SLW, and FSK methods
C_a^p absorption cross-section of a soot primary particle [m^2]
C_a^{agg} absorption cross-section of a soot aggregate [m^2]
d diameter [m]
D_{cx}, D_{cy}, D_{cz} integral over a control angle of the direction cosines relative to x, y and z-axis

$E(m)$	absorption function of the soot refractive index
f_S	soot volume fraction [-]
F	line shape profile [cm]
F_L	Lorentz line shape profile [cm]
g	cumulative *k*-distribution
G	Filter function for LES [m^{-3}]
G_η	incident radiation per unit wavenumber [$W \cdot m^{-1}$]
h	specific enthalpy [J/kg]
H	Heaviside function
I	radiative intensity [$W \cdot m^{-2} \cdot sr^{-1}$]
I_b	Planck function [$W \cdot m^{-2} \cdot sr^{-1}$]
$I_{b\eta}$	blackbody intensity [$W \cdot m^{-2} \cdot sr^{-1}$]
J	Molecular diffusive flux vector for enthalpy [$J.m^{-2}.s^{-1}$]
k	absorption coefficient [cm^{-1}] or the imaginary part of complex refractive index [-]
k^*	absorption coefficient in the FSCK RTE [cm^{-1}]
M	total number of discrete directions (DOM) or control angles (FVM)
m	complex refractive index
n	real part of refractive index [-]
$\boldsymbol{n}$	unit vector normal to the boundary [-]
N	order of the PN approximation
N_g	number of quadrature points for k-distribution methods
N_P	number of primary particles within an aggregate
P	probability
p	pressure [Pa]
p_α	partial pressure of the α^{th} species [Pa]
$\dot{q}''_{R,j}$	net radiative flux in direction *j* [$W.m^{-2}$]
$\boldsymbol{s}$	direction of propagation of radiation intensity [-]
T	temperature [K]
u_j	velocity in the direction j [$m.s^{-1}$]
V	volume [m^3]
w	quadrature weight for the DOM [-]
x_α	mole fraction of the α^{th} species [-]
x_j	mole fraction of the α^{th} species [-]
x, y, z	cartesian coordinates [m]
β	extinction coefficient [m^{-1}]
ε_w	emissivity of the boundary [-]
$\Delta\eta$	narrow band spectral interval [cm^{-1}]
η	wavenumber [cm^{-1}]
η	direction cosine relative to *y*-axis
κ	absorption coefficient [m^{-1}]
κ_P	Planck-mean absorption coefficient [m^{-1}]
λ	wavelength [μm]
μ	direction cosine relative to *z*-axis
ξ	direction cosine relative to *x*-axis
σ_s	scattering coefficient [m^{-1}]
τ	flame optical thickness [-]
Φ	scattering phase function [-]
$\bar{\Phi}$	average scattering phase function [-]

χ particle size parameter [-]
χ_R radiant fraction [-]
ϕ array of variables defining the absorption coefficient, $\phi = \{x_\alpha, p, T, f_S\}$
Ω solid angle [sr]

Subscript
F Fuel
j direction j
l spectral line
S soot
η at a given wavenumber

Superscript
agg aggregate
l *l*th direction (DOM) or *l*th control angle (FVM)
m *m*th direction (DOM) or *m*th control angle (FVM)
p primary particle

Operators
$\langle\phi\rangle$ Reynolds averaged quantity
ϕ' Reynolds fluctuating quantity
$\bar{\phi}$ filtered (or resolved) quantity
ϕ'' subgrid-scale (or residual) fluctuation

1. Introduction

Unlike conductive and convective heat transfer that relies on the transfer of phonons and fluids in materials, radiative heat transfer (RHT) is the transfer of photons and takes place in any media and even in vacuum. The importance of RHT increases very rapidly with increasing temperature due to the exponential dependence of the blackbody radiation intensity on temperature. Therefore, RHT is often the dominant mode of heat transfer in flames, fires, and various combustion systems due to the high temperatures (peak temperatures are typically around 2000 K), the presence of radiatively participating species (mainly CO_2, H_2O, soot, and other particulates in solid fuel flames), and relatively large length scales of such problems, especially in fires and large-scale furnaces and boilers. The importance of RHT in combustion systems has been recognized as early as the late 1940's. The interest of RHT in combustion systems was largely limited to pulverized coal combustion up to the 1980's. The zone method was developed to model RHT in furnaces [1]. RHT in combustion systems and high-temperature reacting flows had not been modeled rigorously for several decades in the combustion and fire communities. In fact, RHT has often been modeled using unjustifiably simple models, namely the optically-thin approximation (OTA), the grey gas (GG) model, or even neglected in some combustion and fire related literature, perhaps for the sole purpose of minimizing the computational cost on RHT. This situation was at least partially due to the underdevelopment of radiative transfer equation (RTE) solvers, radiative property models, and computational fluid dynamics (CFD) as a whole prior to the 1980's. Use of a highly simplified treatment of RHT in combustion and fire modeling may be a consequence of the following two factors. First, RHT appears as a source term in the overall energy conservation equation and is only one of the many complex phenomena that have to be modeled in a combustion problem. Second, accurate modeling of RHT is computationally expensive, since it requires not only solution of the six-variable (three spatial, two angular, and one spectral) integro-differential RTE, but also an adequate representation of the highly spectral dependence of the radiative

properties of combustion products. Solving the RTE in three-dimensional problems even for the GG assumption is computationally demanding, especially if the problems contain scattering particulates and/or are bounded by non-black walls since in these situations iterations are required to achieve converged solution. The computational burden increases significantly when the spectral dependence of combustion products is taken into account, which unfortunately is unavoidable and necessary for accurate modeling of RHT. Additional complexities and computational cost arise in modeling turbulent combustion where the turbulent-radiation interactions (TRI) must be taken into account. Consequently, accurate modeling of RHT through solving RTE coupled with a spectral radiative property model makes the already computationally intensive task of modeling turbulent combustion even more challenging.

The importance of RHT in flames and combustion systems depends on several factors, such as the type of fuel (gaseous, liquid, and solid fuels), combustion condition (flue gas recirculation, oxidizer composition), length scale, residence time, flame temperature, and pressure. In general, RHT tends to reduce the peak temperatures in high-temperature regions but to increase temperatures in low-temperature regions containing radiatively absorbing species, such as CO_2, H_2O and particulates. The relative importance of radiation emission in high-temperature regions and radiation absorption in low-temperature regions is strongly controlled by the system optical thickness in addition to the thermal conditions. Through its impact on the temperature distribution, RHT has a strong influence on kinetically-controlled and highly temperature-sensitive processes, such as soot and NO_x formation and CO and unburnt hydrocarbon emissions. RHT also plays an important role in various near-limit flame phenomena.

With the advance of combustion and flame modeling, such as advanced numerical algorithms, combustion chemistry mechanisms, and turbulence and turbulent combustion models, the importance of accurate modeling of RHT to the overall accuracy of both laminar and turbulent combustion modeling has drawn increased attention recently as evidenced by the gradual adoption of accurate and efficient RTE solvers and nongrey radiative property models, such as WSGG, SLW, and FSCK, in modeling combustion systems and flames. The recent trend of modeling RTH accurately in combustion and flame research has been driven on one hand by the need to understand the importance and develop models of TRI. This is required to more accurately predict the temperature distribution, which is strongly influenced by RHT and is crucial for predicting pollutant formation and emission. The remarkable progress in computer hardware, especially with the widespread adoption of massively parallel computer architecture, has drastically extended the capabilities of CFD and contributed significantly to this progress. On the other hand, there has been rapid progress in numerical methods for solving the RTE in complex geometries and radiative property models of molecular gases, namely CO_2, H_2O, and CO, and combustion products (mixtures of CO_2, H_2O, CO, soot, and particulates) in the last three decades. The majority of the relevant research has been presented at the International Symposium on Radiative Transfer and Eurotherm Seminars of Computational Thermal Radiation in Participating Media. Some of this research has been published in special issues of these conference series in the Journal of Quantitative Spectroscopy and Radiative Transfer. However, the adoption of these advanced numerical methods and radiative property models by the combustion and fire communities has been relatively slow.

Turbulent combustion modeling has remained an active research topic in the combustion community since the 1960's. Several comprehensive reviews have summarized the progress over the last few decades [2],[3]. In turbulent combustion problems, accurate modeling of RHT becomes even more challenging since TRI must be dealt with in addition to the already formidable issues of solving the RTE and adequately modeling the complex spectral

dependence of combustion products. The computationally intensive TRI modeling often accounts for a significant extra burden to the highly non-linear and also computationally expensive turbulent combustion modeling. TRI has received increased research attention in the last two decades as evidenced by an increased number of publications and several reviews on this subject in recent years [4],[5]. Coelho [4] offered a comprehensive overview of the origin and importance of TRI and different approaches used for TRI modeling up to 2007. A more recent review by Modest and Haworth [5] covers broader issues of turbulent combustion modeling ranging from different methodologies (DNS, LES, and RANS), models of turbulence combustion interactions (TCI) in LES and RANS, radiative properties, RTE solvers, and TRI models, to radiative effects in laminar flames and the importance of TRI in different flames and combustion systems.

The advent of new-concept combustion technologies, such as oxy-fuel combustion and flue gas recirculation (FGR), and the need for more accurate temperature modeling to better predict pollutant formation and oxidation, e.g., soot and NO_x, have driven the recent rapid progress in radiative property models in these new applications, especially the weighted-sum-of-grey-gases (WSGG) model. A radiative model is required not only to be acceptably accurate, but also must be sufficiently efficient to be used in coupled numerical modeling of turbulent combustion problems. This is because RHT is only one of many phenomena to be modeled in turbulent combustion, and the CPU time spent on RHT must be kept below a few percent of the overall computing time to make the modeling task tractable. The modern RHT models in combustion and fire modeling and CFD in general are built on several seminal studies, including the RTE solvers (Discrete Ordinates Method (DOM), Finite Volume Method (FVM)), radiative property models (WSGG, Spectral-Line Weighted-sum-of-grey-gases (SLW), and Full-Spectrum Correlated-*k* (FSCK)), and the coupling of WSGG and RTE, and will be reviewed in this article. The rapid progress in RHT modeling over the last three decades has produced abundant choices of RTE solvers and radiative property models to model a wide range of combustion related problems, from laminar flames, internal engine combustion, turbulent flames, to pulverized coal-fired furnaces and boilers. It is important to understand the advantages and disadvantages of these models and methods to make a suitable choice between accuracy and computational efficiency for the problem at hand.

Although the progress in modeling RHT in flames and combustion systems has been reviewed recently by Coelho [4] and Modest and Haworth [5], there have been significant advances in almost all aspects of RHT modeling and applications. This includes, but not limited to, radiative property models, RTE solvers, the effects of non-grey walls, the relative importance of gaseous and particulate radiating components in furnaces, and the understanding of TRI in turbulent non-premixed sooting flames, since the recent review of Modest and Haworth [5]. Therefore, it is the intention of the present article to review and summarize the literature on the importance of RHT in flame and combustion processes and the recent advance in modeling RHT in both laminar and turbulent combustion with an emphasis on modeling RHT in turbulent non-premixed combustion. The outline of the article is as follows. Section 2 concerns the background, including discussions on the coupling between RHT and combustion, the factors affecting RHT, the validity of the common OTA and Grey approximation and some summarizing remarks. The recent progress in RTE solvers is reviewed in Section 3, and Section 4 summarizes the research devoted to the radiative property models of radiating gases and combustion products containing gases and nongrey particulates such as soot, char, and fly-ash. Section 5 discusses TRI. Section 6 discusses the role of RHT in various small-scale flames and fundamental combustion phenomena. Particular attention is paid to the role of RHT in premixed flames under near-limit conditions. Section 7 reviews the recent work on the numerical

modeling of turbulent flames and combustion systems involving advanced radiation models. Finally, some conclusions drawn from this review as well as the perspectives for future works are summarized in Section 8.

2. Background

2.1. Coupling between RHT and combustion

As a heat transfer mechanism, RHT affects the conservation of energy through the divergence of the radiative flux, $\boldsymbol{\nabla \cdot \dot{q}''_R}$ [6]:

$$\frac{\partial(\rho h)}{\partial t} + \frac{\partial\left(\rho u_j h\right)}{\partial x_j} = \frac{Dp}{Dt} + \tau_{ij}\frac{\partial u_i}{\partial x_j} - \frac{\partial J_{q,j}}{\partial x_j} - \frac{\partial \dot{q}''_{R,j}}{\partial x_j} \tag{1}$$

The divergence of the radiative flux represents the local difference in rates between emission and absorption and can be expressed as [6]:

$$\begin{aligned}\frac{\partial \dot{q}''_{R,j}}{\partial x_j} &= \int_{\mathbf{0}}^{\infty} 4\pi\kappa_{\boldsymbol{\eta}} I_{b\eta}\, d\eta - \int_{\mathbf{0}}^{\infty} \kappa_{\boldsymbol{\eta}} \left(\int_{\mathbf{4\pi}} I_\eta\, d\Omega\right) d\eta \\ &= \underbrace{4\pi\kappa_p I_b}_{emission} - \underbrace{\int_0^{\infty} \kappa_\eta \left(\int_{4\pi} I_\eta\, d\Omega\right) d\eta}_{Absorption}\end{aligned} \tag{2}$$

The spectral radiative intensity, I_η, is obtained from solution of the spectral RTE [6]:

$$\boldsymbol{s \cdot \nabla} I_\eta = \kappa_\eta I_{b\eta} - \left(\kappa_\eta + \sigma_{S,\eta}\right) I_\eta + \frac{\sigma_{S,\eta}}{4\pi}\int_{4\pi} \Phi(\Omega' \rightarrow \Omega)\, I_\eta(\Omega') d\eta \tag{3}$$

As discussed in the introduction, the spectral RTE is a six-variable (three spatial, two angular, and one spectral) integro-differential equation, and its solution requires, on one hand, a specific solver and, on the other hand, the knowledge of the spectral radiative properties of the medium, namely the absorption coefficient, κ_η, the scattering coefficient, $\sigma_{S,\eta}$, and the phase function, Φ. The radiatively participating species can be grouped into two classes: non-scattering species, including radiating gases such as CO_2, H_2O, CO, and hydrocarbon fuels, and soot particles and scattering species such as biomass, coal, char and ash particles, or droplets. Although scattering by soot particles in the visible spectrum is important for soot diagnostics, scattering by unagglomerated soot in RHT in the infrared spectrum is generally negligible.

RHT is important in combustion problems owing to the high temperatures (peak temperatures ~ 2000 K in most practical combustion systems). Due to the photon emission nature of thermal radiation, it is ubiquitous. In combustion and fire related problems, thermal radiation emission from high-temperature regions or hot surfaces is in general an inherent heat loss mechanism, while radiation absorption in low-temperature regions or cool surfaces help gain heat. RHT plays the vital role in the long-range transfer of heat for the spread of fires in both confined space [7] and open wildland fire [8], though it is not always the controlling heat transfer mechanism [9]. RHT taking place inherently in combustion systems, open flames, and fires not only modifies the heat transfer process and hence the temperature distribution but also has additional influences on flames and combustion in the following aspects as pointed out by Bedir

and T'ien [10]. First, RHT is the dominant factor affecting the flammability limits in weakly convective flames. Second, radiation heat loss from flames can significantly affect flame stability. Third, radiation can strongly affect the structure and burning rate of diffusion flames by acting as an important heat feedback mechanism to the surface of condensed fuel. In addition, RHT can also become a controlling mechanism in various other flame phenomena under certain conditions, such as ignition, extinction, and flame propagation.

2.2. Factors affecting RHT

The factors affecting RHT can be analyzed by considering the radiant fraction, a metric to measure radiative loss in flames. Let us consider a burner of diameter d_F releasing a fuel of density ρ_F and heat of combustion Δh_c at a velocity u_F into a quiescent atmosphere. The resulting flame volume is denoted as V_{fl}. The radiant fraction can be expressed as:

$$\chi_R = \frac{\dot{Q}_{em} - \dot{Q}_{abs}}{\dot{Q}_{ch}} \tag{4}$$

where $\dot{Q}_{em}$, $\dot{Q}_{abs}$ and $\dot{Q}_{ch}$ refer to the total emission, total absorption and combustion heat release rate of the flame, respectively. These terms can be defined as follows:

$$\dot{Q}_{em} = \int_V 4\pi\kappa_p I_b \, dV \tag{5}$$

$$\dot{Q}_{abs} = \int_V \left[\int_0^\infty \kappa_\eta \left(\int_{4\pi} I_\eta \, d\Omega \right) d\eta \right] dV \tag{6}$$

$$\dot{Q}_{ch} = \rho_F u_F \pi (d_F/2)^2 \Delta h_c \tag{7}$$

The radiant fraction can be re-expressed by introducing the flame volume:

$$\chi_R = \overbrace{\underbrace{\frac{4V_{fl}}{\pi u_F d_F^2}}_{I} \cdot \underbrace{\frac{\dot{Q}'''_{em}}{\rho_F \Delta h_c}}_{II}}^{emission} \cdot \overbrace{\underbrace{\left(1 - \frac{\dot{Q}_{abs}}{\dot{Q}_{em}}\right)}_{III}}^{absorption} \tag{8}$$

where $\dot{Q}'''_{em}$ denotes the total emission per unit flame volume. The right hand side of Eq. (8) is grouped into three terms. The two first terms govern the flame emission whereas the third is associated to flame absorption. They can be interpreted as follows:

- Term I represents a flow residence time. Increasing the residence time enhances flame emission. This explains why radiative emission is generally enhanced in micro-gravity configurations and large-scale combustion problems.
- Term II can be re-written as $4\kappa_p \sigma T_P^4/(\rho_F \Delta h_c)$ where T_p is an emission temperature. It can be interpreted as the inverse of a characteristic radiation cooling time. This term increases with the temperature and the concentration of radiating species of the system.
- Term III represents the flame transparency with the ratio $\dot{Q}_{abs}/\dot{Q}_{em}$ quantifying the part of the flame emission that is re-absorbed within the flame. The flame transparency is reduced as the concentrations of radiating species, pressure and the dimensions of the problem are

enhanced. It is more difficult to model because its quantification requires solving the spectral RTE that is generally a computationally expensive task. Two simplified treatments are generally introduced. The first is the Optically-Thin Approximation (OTA) that consists of neglecting the flame re-absorption (flame transmission is very close to unity). The second approximation, referred to hereafter as the Grey Gas approximation, consists of neglecting the spectral dependence of the radiatively participating species.

2.3. Validity of the OTA and grey gas approximations

The OTA can be applied in small-scale 1D combustion systems operating at atmospheric pressure as long as these systems do not contain radiatively absorbing species in fresh mixtures in premixed flames or the fuel and oxidizer streams in non-premixed flames. The latter point will be discussed in Section 6. The OTA is also reasonable for normal-gravity laminar axisymmetric diffusion flames at atmospheric pressure, including inverse and normal diffusion flames [11]. It was also found reasonable for atmospheric-pressure small-scale micro-gravity flames spreading over thin electrical wires (~ 1 mm) in opposed-flow configuration [12]. However, the OTA becomes questionable for normal laminar coflow diffusion flames at the smoke-point limit [13], where the prediction of the transition from non-smoking to smoking flames and the amount of soot released from the smoking flames were found to be affected by flame reabsorption. It ceases to be valid for high-pressure laminar hydrogen laminar diffusion flames [14] and microgravity axisymmetric coflow laminar diffusion flames [11],[15]. In the framework of lab-scale turbulent jet diffusion flames, the OTA is never a good approximation. Even for the hydrogen flame investigated by Barlow and Carter [16], 20% of flame emission was found to be reabsorbed [17].

The grey gas assumption is also rarely a good approximation to yield acceptable accuracy. As an example, Wang et al. [18] investigated the radiative structure of one of the oxygen-enriched lab-scale propane turbulent jet diffusion flames investigated experientially in Ref. [19]. They found that both non-grey gas and soot modeling are crucial to provide accurate prediction of flame temperature. They also demonstrated that non-grey soot modeling influences flame temperatures in the upstream and the flame-tip region and is essential for accurate predictions of NO. On the other hand, the non-grey treatment of gases was found to weakly affect upstream flame temperatures and NO predictions.

2.4. Summary remarks

The above discussions showed that RHT is an important heat transfer mechanism in combustion systems and flames. Its importance was well summarized in the conclusions of the early review article of Viskanta and Menguç in 1987 [20]: "…*very often radiation plays an important, if not the dominant, role in heat transfer not only in large and intermediate but also in small combustion systems. Neglect of radiation cannot be justified in modeling combustion phenomena*." It was also showed that it is difficult to justify the optically-thin or grey gas/particle approximations even in small-scale systems. The previous analysis demonstrated that RHT may become more important in oxygen-enhanced combustion, elevated pressures, microgravity and large systems and must be accurately modeled for validation of reaction mechanisms and pollutant formation models. This raises questions about the choice of RTE solvers, about the modeling of the radiative properties of participating species and, in turbulent flames, about the modeling of TRI. The state-of-the-art models for these three aspects will be reviewed in Sections 3, 4 and 5, respectively.

3. RTE Solvers

Many methods have been developed for the solution of RHT problems in participating media. Among these, the Monte Carlo (MC) [21],[1], spherical harmonics [22], discrete ordinates (DOM) [23],[24] and finite volume (FVM) [25],[26] methods are the most widely used ones at present for combustion applications. Other methods are available for the solution of RHT problems, but they will not be addressed here.

3.1. Monte Carlo Method

The Monte Carlo method [21] is generally recognized as the most powerful technique to solve radiative transfer problems, allowing the simulation of problems in complex geometries, bounded by surfaces with directionally and spectrally dependent radiative properties, and containing non-grey emitting, absorbing and anisotropically scattering media. The solutions obtained by the MC method are generally considered as a reference, and may be used for benchmark purposes. The statistical error may be easily characterized, allowing quantifying the accuracy of the numerical solution.

The MC method is based on probabilistic concepts to simulate the emission, scattering, reflection and absorption of photons. A large number of photon bundles is fired from random positions in the medium and on the boundaries, and in random directions. The points of emission, the travelling directions, the travelled distances, and the decision on whether a photon bundle hitting a boundary surface is absorbed or reflected, are obtained by drawing random numbers that must satisfy appropriate probability density functions. In the standard forward MC method, the emitted photon bundles are tracked through the medium until they are absorbed or leave the computational domain in the case of open boundaries. A few different formulations of the forward method may be employed [27]. Among them, the energy partitioning strategy, in which the energy of the photon bundles is attenuated by absorption as they travel through the medium, is usually more efficient than the standard formulation, in which the energy of the photon bundles is fully assigned to the cell where absorption occurs.

The backward MC method, also referred to as reverse MC method, is an alternative formulation proposed by Walters and Buckius [28] that is based on the reciprocity principle originally formulated by Case [29]. It is more efficient for certain problems, e.g., if only radiation intensity hitting a small spot and/or over a small range of solid angles is required. In this method, the photon bundles are traced back from the absorption point towards the emission point, allowing for multiple reflections at boundary walls and/or scattering events.

The reciprocity principle [29] is also the basis for the development of the net exchange MC method [30],[31], also referred to as reciprocity MC method [32]. This method uses the reciprocity principle from the point of view of exchanged power and optical path, while only the optical path is used in the backward Monte Carlo method. The photon bundles are followed from the emission to the absorption point and vice-versa.

A rather different MC method was developed by Wang and Modest [33] to calculate radiative transfer in turbulent reactive flows using a PDF transport method [34] for combustion. In this combustion model, the participating medium is represented by discrete stochastic particles, which represent different realizations of the flow, and describe the temperature and chemical composition fields. The interaction between infinitesimal point masses, which correspond to the stochastic particles of the combustion model, and the photon radiation beams, which are

infinitesimally thin, is modeled by assigning effective volumes to the stochastic particles and/or an influence volume to the radiation beams.

Several authors have addressed the acceleration of the ray tracing procedure. Zeeb et al. [35] applied techniques from the field of computer graphics, and reported a reduction in the computational time by a factor of 80 for complex 3D geometries. Mazumder [36] discussed several acceleration methods developed for computer graphics, and proposed a volume-by-volume advancement algorithm, which was found to be faster than previous approaches for 3D boxes, especially when obstructions were placed in the computational domain. Perez et al. [37] investigated the application of these acceleration techniques to participating media by using a binary spatial partitioning method. A space partitioning recursive octree algorithm was also used in [38] for radiative transfer in complex geometries bounding a grey medium. It was found that the octree algorithm reduced the CPU time for wall flux calculations, but not for radiative heat source in comparison to the standard forward MC method with or without energy partitioning.

Soucasse et al. [39] proposed a new MC formulation, referred to as shift method, for radiative transfer in quasi-isothermal, non-scattering media. The ratio of exchanged to emitted powers is very small, since the medium is quasi-isothermal, and so the forward MC method becomes quite slow. This difficulty is overcome in the shift method, which was found to be orders of magnitude more efficient than the forward formulation. The shift method was also compared with the emission and the absorption reciprocity methods, and found to be more efficient for the prediction of wall heat fluxes, but slightly less efficient for the calculation of radiative heat sources.

The tracking of the photons until they are absorbed, particularly in complex geometries and non-homogeneous and non-isothermal media, is a time-consuming task. In these media, the calculation of the locations of absorption or scattering, which requires the inversion of the function that expresses the optical thickness of the medium as a function of the path length, can only be done numerically, rather than analytically. This was the motivation for the development of the so-called null-collision MC algorithm [40]. The idea is to modify the radiative transfer equation (RTE) by adding two new terms that cancel out, namely a new absorption term with a null-collision absorption coefficient, and a purely forward scattering term. The modified extinction coefficient, given by the sum of the original extinction coefficient and the null-collision absorption coefficient, is uniform, thus allowing a straightforward analytical determination of the distance travelled by a photon bundle until absorption or scattering occurs. Galtier et al. [40] applied this concept to the solution of the integral formulation of the RTE using the MC method. The method was further developed by Eymet et al. [41] who proposed a new algorithm to avoid the need of a volumetric mesh, i.e., their MC implementation is independent of the mesh, and applied it to a premixed bluff-body stabilized flame in a combustion chamber.

Another interesting development is the symbolic MC method, which retains some parameters as symbolic variables. A new symbolic MC method based on the null-collision algorithm was reported by Galtier et al. [42], which yields the radiative quantities, such as the radiation intensity, as polynomials of the absorption and scattering coefficients.

Recently, quasi-MC methods [43],[44] were employed to solve RHT problems in 3D participating media, aimed at the improvement of the convergence rate, and therefore the computational efficiency. In these methods, the random numbers are replaced by low-

discrepancy sequences. Sobol sequences were employed by Palluoto et al. [43], while Farmer and Roy [44] used compared three different low-discrepancy sequences: Sobol, Halton and Niederreiter. In both works, the quasi MC method was found to be computationally faster than the traditional MC method in the simulation of turbulent reactive flows. Furthermore, the non-stochastic nature of quasi-MC methods avoids the production of statistical noise in the solution, which can be beneficial in coupling contexts. However, as for MC methods, quasi-MC methods require a large amount of photon bundles to reach convergence.

Despite several different proposals to reduce the computational requirements of the MC method, its main drawback is that it is often computationally expensive in comparison with deterministic methods, particularly in the case of relatively simple problems. In fact, a large number of photon bundles is required to obtain statistically accurate results. In addition, in comparison to other RTE solvers, the MC method is more difficult to adapt to the grid and solution methods for the reacting flow conservation equations. Therefore the software available to solve fluid flow, conduction/convection heat transfer and combustion problems cannot be employed to solve radiation problems using the MC method. New subroutines must be written for this purpose.

3.2. Spherical Harmonic Methods

In the spherical harmonics method [22] the radiation intensity field is written as a truncated series expansion in terms of directional dependent spherical harmonics. The coefficient of each term of the series is a function of the spatial coordinates. The scattering phase function is expressed as a truncated series of Legendre polynomials. These approximations are substituted into the RTE, which is then multiplied by the spherical harmonics of the series expansion and integrated over all directions. In this way, the RTE is transformed into a set of simultaneous partial differential equations. When the spherical harmonics series is truncated after one or three terms, the so-called P1 and P3 approximations are obtained. The former requires the solution of just one partial differential equation. Approximations of order higher than 3 have seldom been employed in the heat transfer community, and only a few works have used the P3 approximation [6]. In fact, approximations of higher order are far more mathematically complicated and the increase of accuracy is slow with the increase of the order of the approximation.

The P1 approximation is by far the most widely used variant in the spherical harmonics approach. The RTE for a grey isotropically scattering medium may be reduced to the following equation (see Modest [6] for details):

$$-\boldsymbol{\nabla}\cdot\left(\frac{1}{3\beta}\boldsymbol{\nabla}G\right) = \kappa(4\pi I_b - G) \tag{9}$$

subject to the following boundary condition, in the case of a diffuse boundary:

$$-\frac{1}{3\beta}\mathbf{n}\cdot\boldsymbol{\nabla}G = \frac{\epsilon_w}{2\,(2-\epsilon_w)}\,(4\pi I_b - G) \tag{10}$$

The P1 approximation often yields fairly accurate solutions at a low computational cost, particularly when the medium is optically thick, the radiation intensity field is nearly isotropic and emission from the medium is dominant. The accuracy decreases in optically thin media and

in strongly anisotropic radiation intensity fields, particularly in multidimensional geometries with large aspect ratios (Modest [6]).

Two modifications of the P1 method have been proposed to increase its accuracy, namely the modified differential approximation (MDA) and the improved differential approximation (IDA). In the MDA, the radiation intensity field is split into two contributions: one component due to radiation leaving from the walls and the other one due to radiation coming from the medium. The former component is determined by dividing the surface of the enclosure into subsurfaces of uniform radiosity and calculating their radiosities by means of a method similar to that commonly employed to calculate radiative transfer in a non-participating medium. The latter component is determined according to the P1 approximation. In the IDA, the integral form of the RTE is employed, leading to the radiation intensity expressed again as the sum of two components. One of them, due to radiation leaving from the walls, is determined as in the MDA. The other, which is related to medium emission and in-scattering, corresponds to the integral of the source function, and is determined by invoking again the P1 approximation. The P1, MDA and IDA methods were compared by Gerardin et al. [45] for 3D emitting, absorbing and linearly anisotropic scattering media. They concluded that the MDA improves the accuracy of P1 in some situations, namely for scattering media and for problems where the radiation field is significantly influenced by radiation from the boundary, but its accuracy is lower than that of the IDA.

Yang and Modest [46],[47] developed a new generic methodology to decompose the PN approximation of the RTE into a set of coupled partial differential equations, which is valid for variable properties and applicable to arbitrary 3D geometries. They employed successive elimination of spherical harmonic tensors, thereby reducing the number of $(N+1)^2$ simultaneous first order partial differential equations of previous PN approximations to $N(N+1)/2$ second-order, elliptic, partial differential equations, which can be solved by standard library packages. A set of generic boundary conditions has also been presented. Although the method can be applied to approximations of any order, only P3 results have been presented. Yang and Modest [46],[47] claimed that the approximation is superior to the discrete ordinates or finite volume methods, for similar order of accuracy, as far as the ray effects and computational efficiency are concerned, particularly for scattering and optically thick media. In both cases, the convergence rate of those methods slows down, while that of P3 remains unaffected.

The set of equations derived in the previous works [46],[47] is rather complicated for spatially varying absorption and anisotropic scattering. Modest [48] reduced the complexity of the formulation for the case of isotropic scattering and used a self-consistent set of boundary conditions derived from the original set of Marshak's boundary conditions. This formulation, which reduces to $2(N+1)/4$ simultaneous equations in two-dimensional problems, was implemented in OpenFOAM [49]. It was found that while the P3 approximation is significantly more accurate than P1, the P5 approximation yields only a slight improvement in accuracy over P3, which is hardly justifiable regarding the increased computational effort. A simplified formulation for 2D axisymmetric problems, which also involves $2(N+1)/4$ simultaneous partial differential equations, was presented by Ge et al. [50], and also implemented in OpenFOAM. Additional refinements of this work were reported by Ge et al. [51] who derived a 2D Cartesian version of the higher-order PN method, extended the boundary conditions to allow for nonblack and mixed diffuse-specular surfaces, and to deal with specified radiative flux at the walls and for symmetry/specular reflection boundaries.

The P1 approximation is computationally cheap and may be easily incorporated in codes for the solution of the reactive flows. The P3 approximation yields a system of partial differential equations, being more computationally demanding and requiring more effort to integrate in combustion codes, since those equations are strongly coupled and are mathematically different from the transport equations that govern conservation of for mass, momentum, energy and chemical species.

3.3. Discrete Ordinates and Finite Volume Methods

The DOM [23],[24] and the FVM [25],[26] are two somewhat similar techniques often used to solve the RTE. These methods often yield relatively accurate results for a wide range of problems with moderate computational resources. Strictly speaking, the terminology DOM and FVM refers to how the angular discretization of the RTE is carried out, and does not reflect how the spatial discretization is performed. Indeed, both methods usually rely on the finite volume method to spatially discretize the RTE, even though a few different spatial discretization procedures have been employed in the case of the DOM. As far as the angular discretization is concerned, the DOM solves the RTE for a set of discrete directions, which span the total solid angle range of 4π steradians around a point in space, and approximates the integrals over solid angles by means of a numerical quadrature rule. In contrast, in the FVM the RTE is integrated over the control angles that arise from the angular discretization of the total solid angle of 4π. It is assumed that the radiation intensity is constant within a control angle, but its direction is allowed to vary within that angle.

In the DOM, the discrete form of the RTE for a Cartesian coordinate system and for the step scheme may be written as follows for a discrete direction m (see Coelho [52] for a detailed derivation of this equation), where m ranges from 1 to the total number of discrete directions, denoted by M:

$$\begin{aligned}\left[|\xi^m|A_x + |\eta^m|A_y + |\mu^m|A_z + \beta V - \frac{\sigma_s}{4\pi} w_m \Phi(s^m, s^m) V\right] I_p^m \\ = |\xi^m| A_x I_{x,in}^m + |\eta^m| A_y I_{y,in}^m + |\mu^m| A_z I_{z,in}^m + \kappa I_{b,P} V \\ + \frac{\sigma_s}{4\pi} V \sum_{\substack{l=1 \\ (l \neq m)}}^{M} \Phi(s^l, s^m) I_p^l \, w_l\end{aligned} \tag{11}$$

In the FVM, considering once again a Cartesian coordinate system and the step scheme, the discrete form of the RTE for the mth control angle (see again Coelho [52] for a detailed derivation of this equation), where m ranges from 1 to the total number of control angles, denoted by M, is written as:

$$\begin{aligned}\left[|D_{cx}^m|A_x + \left|D_{cy}^m\right|A_y + |D_{cz}^m|A_z + \beta V \Delta\Omega^m - \frac{\sigma_s}{4\pi} \Delta\Omega^m \Delta\Omega^m \bar{\Phi}^{mm} V\right] I_p^m \\ = |D_{cx}^m| A_x I_{x,in}^m + \left|D_{cy}^m\right| A_y I_{y,in}^m + |D_{cz}^m| A_z I_{z,in}^m + \kappa I_{b,P} V \Delta\Omega^m \\ + \frac{\sigma_s}{4\pi} V \sum_{\substack{l=1 \\ (l \neq m)}}^{M} \bar{\Phi}^{lm} I_p^l \, \Delta\Omega^l \Delta\Omega^m\end{aligned} \tag{12}$$

where

$$D_{cf}^{m} = \int_{\Delta\Omega^m} \mathbf{s}\cdot\mathbf{n}_f \; d\Omega^m \tag{13}$$

$$\Delta\Omega^m = \int_{\Delta\Omega^m} d\Omega^m \tag{14}$$

$$\bar{\Phi}^{lm} = \frac{\int_{\Delta\Omega^l}\int_{\Delta\Omega^m}\Phi\left(s^l, s^l\right)\mathrm{d}\Omega^m\mathrm{d}\Omega^l}{\Delta\Omega^m\Delta\Omega^l} \tag{15}$$

The radiation intensities for different directions or control angles are coupled via the in-scattering term (last term of the right hand side of Eqs. 11 and 12) and, if the boundary surfaces are not black, via the boundary conditions.

The accuracy of the DOM and FVM depends on the spatial and angular discretization methods employed. The step scheme often leads to false scattering (similar to false diffusion in CFD), while the diamond scheme, which corresponds to the central difference scheme in CFD, is unbounded and may yield unphysical results. High order spatial discretization schemes effectively overcome the limitations of the step and diamond schemes. The most popular schemes are based either on the normalized variable diagram boundedness criteria or on the total variation diminishing criteria [53].

The angular discretization in the DOM is usually based on a few recommended guidelines, while in the FVM it is generally carried out using the piecewise-constant angular discretization procedure. The set of discrete directions in the DOM should be invariant to rotations of 90° about the coordinate axes, the quadrature weights should be positive, and the lowest order moments of the direction cosines should be exactly satisfied, particularly the moments of order zero, one and two. These rules still leave much freedom in the selection of the quadrature, and therefore several different possibilities are available [54], the most widely used ones being the SN quadrature.

Both the DOM and the FVM suffer from ray effects, which arise from the angular discretization, and result from the approximation of the radiation intensity, which is a continuously varying function of the direction, by a piecewise constant function of the direction. Still, ray effects may be mitigated somewhat in the FVM, because the variation of the direction of the radiation intensity within a control angle is taken into account (see Eq. 13). While ray effects may be reduced by increasing the number of discrete directions, a very fine angular refinement is often needed to successfully reduce them, but this has an adverse impact on the computational requirements. Several methods have been proposed to diminish the errors due to ray effects, but no general and effective solution is available. If the ray effects arise from discontinuities or sharp gradients in the boundary conditions, the modified DOM [55], which is based on the decomposition of the radiation intensity employed in the MDA, is able to overcome this problem. However, the calculation of the component of the radiation intensity coming from the boundaries requires the numerical solution of a few integrals, in the case of Cartesian coordinates, or the use of another method, e.g., the zone or the Monte Carlo method, in the case of complex geometries. In the latter case, there is a major increase in complexity and CPU time in comparison with the standard formulation.

It was found that the errors due to ray effects and false scattering have opposite effects and tend to compensate each other [56]. In fact, false scattering smooths, and ray effects enhances, discontinuities or gradients of the radiation intensity field. As a consequence, the increase of

the solution accuracy requires the simultaneous reduction of the errors due to false scattering and ray effects. Accordingly, both spatial and angular refinement should be carried out simultaneously. Otherwise, if only the spatial grid or the angular discretization are refined, the solution accuracy might decrease.

Classical numerical methods for the solution of the system of discretized equations may be applied to solve the discretized equations in the DOM and FVM. It turns out that radiation propagates along straight lines in media with uniform refractive index, and this implies that the radiation intensity at a grid node depends only on the radiation intensity at upstream grid nodes, provided that the in-scattering is treated as a source term. Hence, the Gauss-Seidel method is widely used. In this method, the radiation intensity is calculated by sweeping all the control volumes by lines or columns, starting from a control volume at one of the corners of the computational domain. This corner is selected according to the direction under consideration, in such a way that the radiation propagates from the cell faces of that control volume that are coincident with the boundary of the domain to the interior of the domain. In general, the solution algorithm is iterative. Other solution algorithms may be employed, such as Krylov subspace iterative methods.

A comprehensive review of the DOM and FVM is available in Coelho [57]. In the last few years, several works have been published aiming at the improvement of accuracy or reduction of the computational requirements of these methods. The DOM does not guarantee energy conservation in the case of anisotropic scattering, i.e., the integral of the phase function over the sphere may be different from the actual value of 4π. A simple correction factor can be used to overcome this problem, but it may change the shape of the scattering phase function when the asymmetry factor of the phase function is large. Several methods have been proposed to simultaneously satisfy conservation of energy and maintain the shape of the phase function [58],[59]. Modifications of the angular discretization procedure have been used to reduce the ray effects, namely by averaging the computed solution for several reference frame orientations [60], by employing a goal-based angular adaptivity method [61] or a goal-oriented regional angular adaptive algorithm [62]. The application to problems with specular reflection was addressed in Refs. [63],[64].

The DOM and FVM provide a good compromise between accuracy and computational requirements for many problems, being quite popular in heat transfer and combustion applications. They are both easily included in combustion codes, since the discrete equations are mathematically similar to those that describe fluid flow, energy and species transport, and the same solution methods can be employed.

A comparison of the three methods described above is illustrated in Fig. 1 [47]. It shows the normalized incident heat flux on the top wall of a two-dimensional square enclosure of side length L and bounded by black and cold walls, except in the mid-section of length d_h of the bottom wall, whose temperature is T_h. The results shown in Fig. 1 were obtained for d_h/L=0.2 and for a pure, isotropically scattering medium with an optical thickness of unity based on the enclosure side length. The Monte Carlo solution may be considered as almost exact. The P3 method yields smooth profiles, but the heat flux is overpredicted by about 40% at x=0. In contrast, the FVM profiles exhibit unphysical oscillations due to ray effects caused by the discontinuity in the temperature at the bottom boundary. If grid refinement is carried out for the same angular discretization (4 × 8), the amplitude of the oscillations increases and the solution becomes worse. Similarly, if the angular discretization is refined for the same mesh (10 × 10), the solution does not improve. Both spatial and angular refinement should be carried out

simultaneously, as discussed by Raithby [56], but ray effects for this problem can only be mitigated by using very fine spatial and angular discretization, which is too computationally demanding. It is worth to point out that this is a test case with particularly severe ray effects, because only a small region in the boundary is hot and there is an abrupt temperature discontinuity at the edges of that region. An alternative that would effectively remove the ray effects and yield an accurate solution would be the modified DOM or modified FVM [55],[57].

The methods described above are also compared in Fig. 2 for combined steady state, laminar, natural convection and radiation in a two-dimensional square enclosure [65]. The top and bottom walls are adiabatic, and the left and side walls are maintained at 310 K and 290 K, respectively. All the walls are black, and the medium is assumed to be grey and does not scatter. The results shown in Fig. 2 were obtained for a Rayleigh number (Ra) of 10^4 and a Planck number (Pl) of 0.1, using a mesh with 61×61 control volumes and, in the case of the FVM, 4×8 control angles. They represent the variation of the Nusselt number along the hot wall, which was defined as $q\,L/k\,\Delta T$, where q is the sum of the convective and radiative heat fluxes, L the side length, k the thermal conductivity of the medium and ΔT the difference between the temperatures at the hot and cold walls. The DOM and FVM predictions are very close to the Monte Carlo reference solution, even though a few discrepancies are visible for the FVM in the cases of an optical thickness of τ=0.1 and τ=1. The P1 approximation consistently yields poor predictions, while P3 performs well for τ=5 and τ=10, but still deviates significantly from the reference solution for τ=0.1 and τ=1. Figure 2 also includes results obtained using the simplified spherical harmonics (SP) method [66], which was not mentioned above.

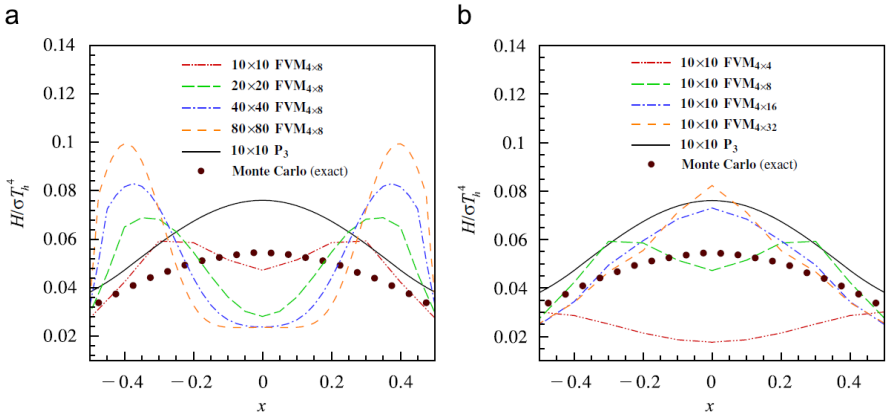

Figure 1. Incident heat flux on the top wall of a square enclosure bounded by black and cold walls, except in a small region in the middle of the bottom wall. (a) Influence of the spatial discretization in the FVM; (b) Influence of the angular discretization in the FVM.

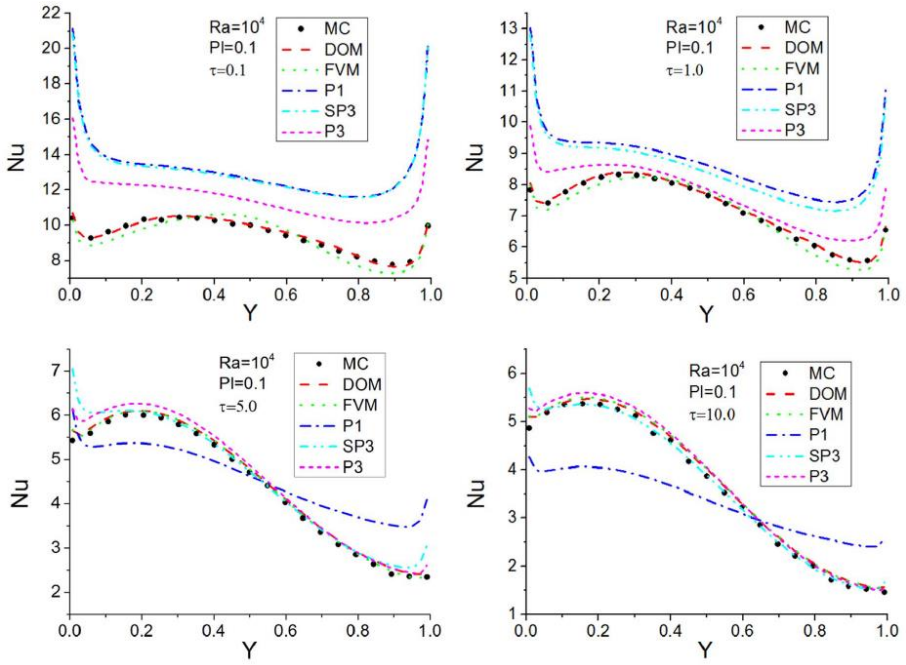

Figure 2. Nusselt number along the hot wall of a two-dimensional square enclosure for Ra = 10^4 and P_l = 0.1.

The choice of the RTE solver is mainly dictated by the application and the computational effort that can be accepted. Very few works were devoted to extensive comparison of MC, PN and DOM or FVM in coupled calculations of combustion systems. A notable exception is the work of Pal et al. for turbulent jet flames [67]. They compared radiative models involving different gas radiative property models and RTE solvers for the RANS simulation of the Sandia flame D and two other optically thicker flames designed from the Sandia flame D by scaling up the burner diameter by a factor of 4 with or without soot. The combustion model was a transported PDF approach whereas soot volume fraction was introduced through simple state relationships. For the RTE solvers, the authors compared the Photon Monte Carlo (PMC) method, developed by Wang et al. [33], the P1, P3, and the FVM with 16 × 4 control angles. For the optically-thin Sandia flame D all the RTE solvers were found to provide accurate predictions and, in such configuration, the P1 is recommended due to its simplicity. For the optically thicker flames, the P3 and FVM were found to provide predictions comparable with those of the PMC with the P3 being significantly more computationally efficient.

4. Radiative properties of particles and gas

4.1. Gas radiative property models

4.1.1. General comments about gas-radiation interactions

Interactions between gases and electromagnetic radiation occur at the molecular scale. They are due to exchanges of energy quanta between molecules and the radiation field. Gas spectra are comprised of millions of spectral lines, each of which is associated with a transition between particular energy levels of the molecule (pairs of rotational and vibrational levels with distinct sets of quantum numbers are considered in the infrared), as described theoretically in [68].

Each spectral line is characterized by: 1) a location in the spectrum (its line center η_l, whose value is proportional to the difference between the energy of the two states involved in the

radiative transition), 2) a value of the integrated area under the spectral line (called its line strength, S_l) and 3) a profile $F(\eta - \eta_l)$, that accounts for the physical mechanisms (collisional, Brownian motion, etc.) that drive the shape of the spectral lines. In most combustion applications, it is reasonable to treat spectral line profiles as Lorentz, $F(\eta - \eta_l) = F_L(\eta - \eta_l)$, i.e., related to collisions between the gaseous molecules. Because the Lorentz model over-predicts the absorption in the line wings, these profiles are, in practice, truncated at some reasonable distance from line center. With these notations, the absorption coefficient of the gas at some wavenumber η is the sum of the contributions of all spectral lines in the spectrum:

$$\kappa_\eta = xp \sum_{lines} F_L(\eta - \eta_l) \tag{16}$$

where x is the molar fraction of absorbing gaseous species and p the total pressure of the gas. Figure 3 depicts small portions of absorption spectra for CO_2 at atmospheric pressure and various temperatures. It is obvious from this figure that 1) gases are highly non-grey media, as values of their spectral absorption coefficient vary over several orders of magnitude, and 2) gas spectra are strongly dependent on temperature with the appearance of the so-called hot lines. These lines are imperceptible at ambient temperature and become of increasing importance as the temperature grows. As such, temperature affects strongly the number of lines to account for accurate predictions. Pearson et al. illustrated this behavior [69]. They showed that there are 202,228, 78,960 and 1706 important lines for H_2O, CO_2 and CO at 400K, respectively. These numbers reach 1,697,210, 7,903,720 and 8633 at 1,500K and 60,165,500, 8,370,444, and 23,428 at 3,000 K. From Fig. 3, one can notice that the dependence of absorption coefficients on temperature cannot be represented as a simple linear relationship between the spectra. In other words, gas spectra in distinct states are not scaled, viz. the spectral and local (through the local properties of the gas) dependencies of the absorption coefficient cannot be treated independently.

Figure 4 illustrates the influence of total pressure on gas spectra at a fixed gas temperature (1,500 K): collisions between molecules lead to a broadening of the spectral lines that reduces the amplitude of rapid variation of the absorption coefficient. However, even at high pressure (30 atmospheres is the maximum considered in this figure), gases cannot be reasonably considered as grey media. Changes in total pressure have significant effects on RHT [70],[71]. Chu et al. [72],[73] performed 1D and 2D axisymmetric decoupled RHT with several gas radiative property models. They showed that pressure affects gas radiation predominantly through an increase in gas density (proportional to the product xp in Eq. 16) whereas the broadening of spectral lines with increasing pressure, although significant as illustrated in Fig. 2, has a small influence on gas radiation transfer. Their calculations were limited to configurations with characteristic dimensions of the order of 1 m and this result has to be verified for media at larger physical scales.

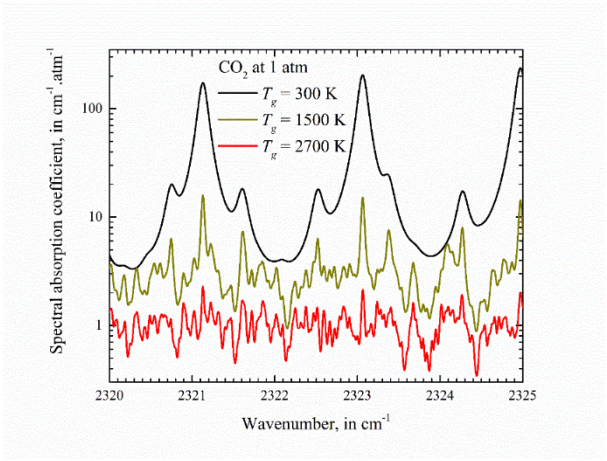

Figure 3. portions of CO_2 spectra at 1 atm and various temperatures – LBL data from Ref. [70]

Figure 5 depicts two absorption spectra of CO_2 at atmospheric pressure. The band structures clearly appear in this figure. Spectra are represented with respect to the wavenumber, which is the inverse of the wavelength of radiation. This kind of representation is common in spectroscopy as the wavenumber relates directly with the outputs of Fourier Transfer spectrometers. This figure introduces the concept of a narrow band that has a band interval of the order of 25 cm^{-1} over which the blackbody intensity as well as the radiative properties of particles can be assumed constant.

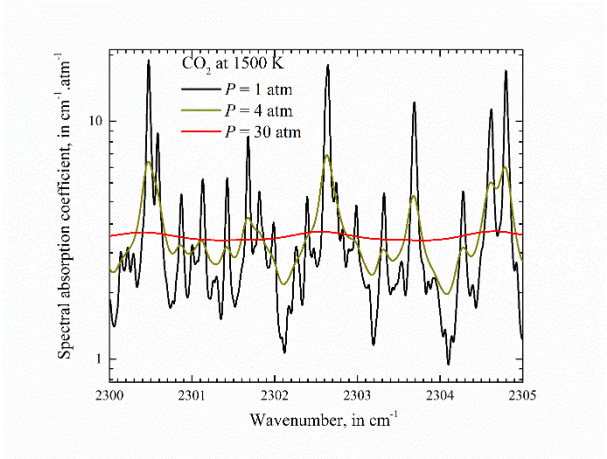

Figure 4. Portions of CO_2 spectra at 1500 K and various pressures– LBL data from Ref. [70].

The simplest and arguably most accurate method to treat radiative transfer problems in gases is to solve the RTE at high spectral resolution, rigorously accounting for the complex variation of absorption properties with wavenumber. This approach is referred to as Line-by-Line (LBL) integration, since it intends to resolve individual spectral lines. LBL methods are the reference for decoupled RHT with the availability of accurate high-temperature high-resolution spectroscopic databases such as HITEMP 2010 [74]. Typically, the spectral resolution in LBL simulations of gas radiative transfer is 0.01 cm^{-1}, which requires one to solve approximately 10^6 RTE to cover the entire spectrum of interest for RHT. Therefore, LBL is extraordinarily time consuming and cannot reasonably be used for RHT calculations in multidimensional-coupled simulations. Presently, even with recent advances in computer resources, approximate methods remain the most relevant choices in practical engineering applications.

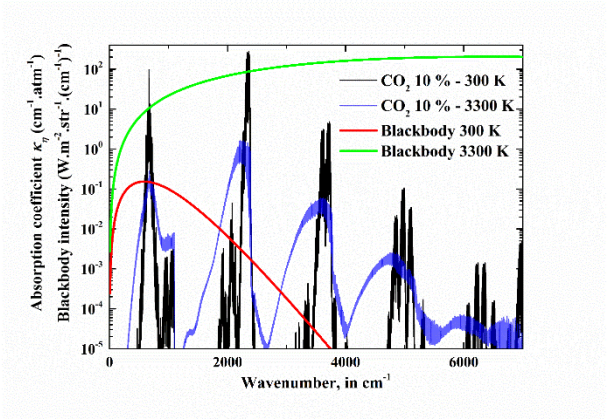

Figure 5. CO_2 spectra at distinct temperatures over the full spectrum– LBL data from Ref. [70].

Approximate gas radiative property models can be classified based on their spectral resolution. Narrow band models such as the Statistical Narrow Band (SNB) and the Narrow Band Correlated-*k* (NBCK) are known to be accurate [75] in usual configurations. However, SNB models cannot be used together with arbitrary RTE solvers, which limits strongly its use in practical applications. The NBCK does not suffer from this drawback but is also probably much too time consuming for coupled RHT problems [73]. The NBCK model was degraded at the wide-band resolution, leading to the Wide Band Correlated-*k* [73],[76]. This model was found to provide NBCK accuracy for spectrally integrated radiative outputs and was applied to the simulation of turbulent jet diffusion flames [77]. Models at the resolution of the full spectrum are referred to as global methods in the literature and include the Weighted-Sum-of-Grey-Gases (WSGG) [78], the Spectral Line Weighted-sum-of-grey-gases (SLW) [79]-[82] the Absorption Distribution Function (ADF) [83] and the Full-Spectrum Correlated-k (FSCK) [84] methods. The WSGG is the most popular gas radiation model for combustion simulations due to its simplicity and ease of implementation. Significant efforts were made over the last decade to update the WSGG parameters from accurate spectroscopic databases and these recent versions have been found to provide reasonably accurate engineering predictions for situations representative of actual combustion problems [78],[85],[86],[87]. Nevertheless, the WSGG model has limitations inherent to its formulation. In particular, it is difficult to deal with general gas mixtures (and particles) where the mole fraction ratios of the participating components are not constant without complicating the model and introducing loss in its computational efficiency [88]. On the other hand, SLW and FSCK methods, which are based on the *k*-distribution concept, are generally more accurate than the WSGG [72],[73],[76],[89],[90] and have benefitted from extensive developments over the last twenty years that make them very attractive for coupled simulations of combustion problems. Both the NBCK and the global models may be readily incorporated in the RTE solvers addressed in section 3, namely MC, P1, P3, DOM and FVM.

k-distribution methods, namely the NBCK and the FSCK will be the focus of this review, although the FSCK and SLW methods are fundamentally identical, and produce identical results when implemented in the same way. The *k*-distribution concept will be first introduced at the narrow band resolution before being extended to the full-spectrum.

4.1.2. Principle of narrow band *k*-distribution methods

As shown in Figure 1, due the strong variation of absorption coefficient with wavenumber (inverse of the wavelength of the radiation), a given value of κ_η is encountered many times over

a spectral interval. The primary idea behind *k*-distribution methods is to group spectral intervals with identical (or similar) values of κ_η. This can be done by defining the probability of encountering inside a narrow band of spectral width, $\Delta\eta$, a value of the spectral absorption coefficient lower than some prescribed value *k* as:

$$g(k) = \mathrm{P}(\kappa_\eta < k) = \frac{1}{\Delta\eta} \int_{\Delta\eta} H(k - \kappa_\eta) d\eta \tag{17}$$

With this definition, the mean value of any function *f* of the absorption coefficient (including the emissivity or transmissivity, or more interestingly, the integral solution of the RTE) can be written as the expectancy of this function with respect to the probability measure Eq. (17):

$$\frac{1}{\Delta\eta} \int_{\Delta\eta} f(\kappa_\eta) d\eta = \int_0^{+\infty} f(k) dg(k) \tag{18}$$

As the function $g(k)$ represents the probability of encountering inside the band a spectral value of the absorption coefficient lower than *k*, it is strictly increasing and thus invertible, and takes on values in the interval $[0,1]$. These properties allow Eq. (18) to be rewritten as:

$$\frac{1}{\Delta\eta} \int_{\Delta\eta} f(\kappa_\eta) d\eta = \int_0^1 f[k(g)] dg \tag{19}$$

where $k(g)$, which is an absorption coefficient representative of the true absorption spectrum in a reorganized spectral scale (sometimes called pseudo-spectral), is the inverse of the function $g(k)$.

The main advantage of the formulation of Eq. (19) compared to its equivalent Eq. (18) is that Eq. (19) involves an integral between 0 and 1 that can be readily approximated with high accuracy through numerical quadratures with few quadrature points (typically of the order of N_g=10):

$$\frac{1}{\Delta\eta} \int_{\Delta\eta} f(\kappa_\eta) d\eta = \sum_{i=1}^{N_g} f[k(g_i)] \omega_i \tag{20}$$

where ω_i and g_i are, respectively, the weights and nodes of the numerical quadrature at order N_g over the interval $[0,1]$. Gauss-Legendre or Gauss-Lobatto quadratures are the most usual numerical schemes encountered to generate these weights and nodes (quadrature points).

4.1.3. Extension to the Full Spectrum

The narrow band *k*-distribution approach described in the previous subsection can be extended to the full spectrum by simply replacing the definition of the probability law Eq. (17) by a formulation more suited to this distinct though similar problem. Accordingly, over the full spectrum, it is common to replace Eq. (17) by:

$$g(k,\phi,T_b) = \mathrm{P}\left[\kappa_\eta(\phi) < k\right] = \frac{1}{I_b(T_b)} \int\limits_{[0,+\infty]} H\left[k - \kappa_\eta(\phi)\right] I_{b\eta}(T_b) d\eta \tag{21}$$

where $I_{b\eta}(T_b)$ is the blackbody radiative intensity provided by the Planck function evaluated at some prescribed temperature T_b and $I_b(T_b) = \frac{\sigma T_b^4}{\pi} = \int_0^{+\infty} I_{b\eta}(T_b) d\eta$ its integral over the full spectrum.

It can be noticed that as soon as this definition of probability law is made, all subsequent relationships for narrow bands, viz. Eqs. (18-20), remain valid over the full spectrum with minor changes.

The main advantage of this method is thus to allow the approximation of any function of the absorption coefficient, that would require many thousands of spectral components at high spectral resolution, by a sum over a few components ($N_g \sim 10$ and equal to the order of the quadrature used for the calculation). A large gain in terms of computational time can thus be achieved by application of the Full Spectrum *k*-distribution method [91],[92].

4.1.4. Extension to non-uniform gas

Up to now, the principle of *k*-distribution methods in isothermal, homogeneous (uniform) gases has been described. In most cases of practical interest, gaseous media are characterized by spatial gradients of temperature and species concentrations. Treating such problems is complicated because, as noticed previously, the spectra are strongly dependent on the local thermophysical properties of the gas, such as temperature, composition and pressure. Adaptation and assumption in the previous relationships are thus required to treat these more general configurations. They are detailed and explained in the following references [68],[93] Only the main ideas and corresponding results are provided here for brevity.

The main idea to extend *k*-distribution methods from uniform to non-uniform media consists in assuming that the spectra for the same molecule in different thermophysical states are related by a functional (correlated, [84]) or statistical (comonotonic, [94]) relationship that preserves spectral intervals in such a way that the following equality between probability functions holds:

$$g(k_1,\phi_1,T_b) = \mathrm{P}\left[\kappa_\eta(\phi_1) < k_1\right] = \mathrm{P}\left[\kappa_\eta(\phi_2) < k_2\right] = g(k_2,\phi_2,T_b) \tag{22}$$

Here, indices 1 and 2 refer to absorption coefficients related to thermophysical states $\phi_1 = \{p_1, T_1, x_1\}$ and $\phi_2 = \{p_2, T_2, x_2\}$, respectively. The same relationship is then assumed to remain valid for any pair of thermophysical states, allowing extension of the present idea to any configuration.

In the case of narrow bands, solving the implicit equation Eq. (22) (that does not depend on T_b in the case of narrow bands) is the basis of the so-called NBCK method. Over the full spectrum, the problem is a bit more complicated because distribution functions $g(k,\phi,T_b)$ depend, from their definition, on the Planck temperature T_b. Subject to the choice of T_b, various methods can be constructed. It was shown in Ref. [95] that a total of eight distinct possible versions can be formulated. Some of them do not preserve the Planck-mean absorption coefficient of the gas, which introduces error since this coefficient characterizes the emission spectrum. Described

below are two versions of the method that preserve Planck mean absorption coefficients. Predictions using these two methods are compared later in this paper in actual RHT calculations in flames.

4.1.5. FSCK (Cai and Modest's scheme, [96])

The FSCK method [91] requires first the definition of a single reference state of the gas, which is used to reorder the wavenumber axis. Then, over this reordered wavenumber scale, gas spectra in distinct states are assumed to be related through an increasing function. This function does not need to be specified explicitly, but rather, is defined implicitly through a relationship of the form of Eq. (22). Notice that the definition of the reference state required for this method can only be made through intuitive reasoning (Gas spectra are never rigorously related through any kind of functional relationship; only cases of single spectral lines can be properly treated this way.) Many methods (such as the ADF method, for example) suffer from the same constraint.

Modest recommends that the gas reference state be determined by volume averaging the mole fractions of radiating species and by considering a blackbody emission-averaged temperature as reference temperature [6]. The stretching factor, $a(g_0)$, is then defined [6] as $a(g_0) = \frac{dg(k_0,\phi_0,T)}{dg_0(k_0,\phi_0,T_0)}$ (see Eq. 23). Here the subscript 0 refers to the reference state. The Cai and Modest scheme to determine the absorption coefficient in Eq. (23) can be summarized as follows [96]: i) determine k_0 from $g(k_0,\phi_0,T_0) = g_0$ where g_0 is a given quadrature point ; ii) determine $g(k_0,\phi_0,T)$ using k_0, and iii) compute k^* by solving $g(k^*,\phi,T) = g(k_0,\phi_0,T)$.

4.1.6. RC-FSK

The Rank Correlated FSK (RC-FSK) [92] method (developed from its predecessor, the RC-SLW model [97]) does not require the arbitrary definition of the reference state of the gas. It has been shown that the RC-FSK and RC-SLW methods are theoretically identical, and produce identical predictions if the same numerical implementation is employed [92]. This method is also founded on a relationship between gas spectra of the form of Eq. (22) but, unlike the FSK or ADF methods which assume a relationship between absorption coefficients in distinct states, in the RC-FSK method (or equivalently RC-SLW), a relationship between spectral intervals is used. This makes the RC-FSK/RC-SLW models different from other correlated methods when applied in discrete form, viz. together with a formula such as Eq. (22), even if all these techniques converge to the same limit for an infinite number of grey gases (which are never used in practice). RC-FSK/RC-SLW methods thus provide results that differ from other correlated methods, even when all parameters (reference state where applicable, blackbody source temperature T_b, number of grey gases) are fixed for all techniques. The RC-FSK scheme can be summarized as follows: i) solve $g(k^*,\phi,T_b) = g_0$ in order to get k^* and to compute $g(k^*,\phi,T)$ to determine the stretching factor defined as $a(g_0) = \frac{\partial g[k(g_0,\phi,T_b),\phi,T]}{\partial g_0}$. Although T_b can be selected arbitrarily, it is generally taken as equal to the reference temperature, T_0 [97],[92].

In both the FSCK and RC-FSK models the corresponding RTE is written as a function of the distribution function $k(g)$ as:

$$\frac{dI(g)}{ds} = k(g)a(g)I_b(T) - k(g)I(g) \tag{23}$$

This form of the RTE is typical of global models and, indeed, is the same equation used for the more classical and more rudimentary WSGG model.

However, as discussed previously, the FSCK and RC-FSK methods described use different approaches to evaluate the weights $a(g)$ involved in the RTE, Eq. (23). These weights play a role similar to those encountered in the WSGG model. However, based on the evaluation of absorption coefficients through a relationship of the form of Eq. (23), the absorption coefficients in RC-FSK/RC-SLW methods depend on the local thermophysical state of the gas encountered along radiation paths. They are thus more representative of the true physics than those used in the WSGG model. This can be clearly seen in Figure 1 (absorption coefficients are strongly dependent of the gas state, and this dependence is neglected in the WSGG, even if this kind of model is presently among the most widely used in coupled combustion calculations).

A comparison of predictions made using the FSCK (Cai and Modest implementation [96]) and the RC-FSK (RC-SLW) model for a one-dimensional problem simulating the temperature and mole fraction profiles that might be encountered in a diffusion flame was reported in Ref. [92]. The layer was 1 m in width at a total pressure of 1 atm, bounded by black walls and filled with water vapour of varying concentration with the remainder nitrogen. The temperature and H_2O mole fraction profiles were given by:

$$T(x) = \frac{(T_{max} + T_{min})}{2} + \frac{(T_{max} - T_{min})}{2} cos\left[\frac{2\pi}{L}(x - L/2)\right] \tag{24}$$

and

$$x_{H2O}(x) = \frac{(x_{H2O,max} + x_{H2O,min})}{2} + \frac{(x_{H2O,max} - x_{H2O,min})}{2} cos\left[\frac{2\pi}{L}(x - L/2)\right] \tag{25}$$

Two cases were investigated featuring moderate and extreme mole fraction and temperature differences, and corresponding average temperature and average mole fraction in the layer: 1) Case A: T_{min} = 300 K, T_{max} = 1300 K, $x_{H2O,min}$ = 0.1, $x_{H2O,max}$ = 0.2 (ΔT = 1000 K, T_{ave} = 800 K, Δx_{H2O} = 0.1, $x_{H2O,ave}$ = 0.15) and 2) Case B: T_{min} = 300 K, T_{max} = 2300 K, $x_{H2O,min}$ = 0.1, $x_{H2O,max}$ = 0.4 (ΔT = 2000 K, T_{ave} = 1300 K, Δx_{H2O} = 0.3, $x_{H2O,ave}$ = 0.25).

FSCK and RC-FSK predictions were compared with benchmark line-by-line spectral integrations carried out using the HITEMP 2010 spectroscopic database, which was also used to generate the FSCK and RC-FSK model parameters. The spatial average temperature was used as the reference temperature in the FSCK model predictions.

Figure 6 illustrates the predictions for local net radiative flux divergence $Q(x)$ in the layer and the local error relative to the line-by-line benchmark. The local error, $LE(x)$ is defined as the absolute difference between FSCK or RC-FSK model and line-by-line benchmark prediction of flux divergence normalized by the absolute maximum benchmark prediction. The figure illustrates that while both the FSCK and RC-FSK model yield very good predictions for both

moderate and extreme differences in gas temperature and mole fraction, the accuracy of the RC-FSK model is somewhat better. Further, as stated previously, unlike the FSCK method, the RC-FSK model requires no gas reference state.

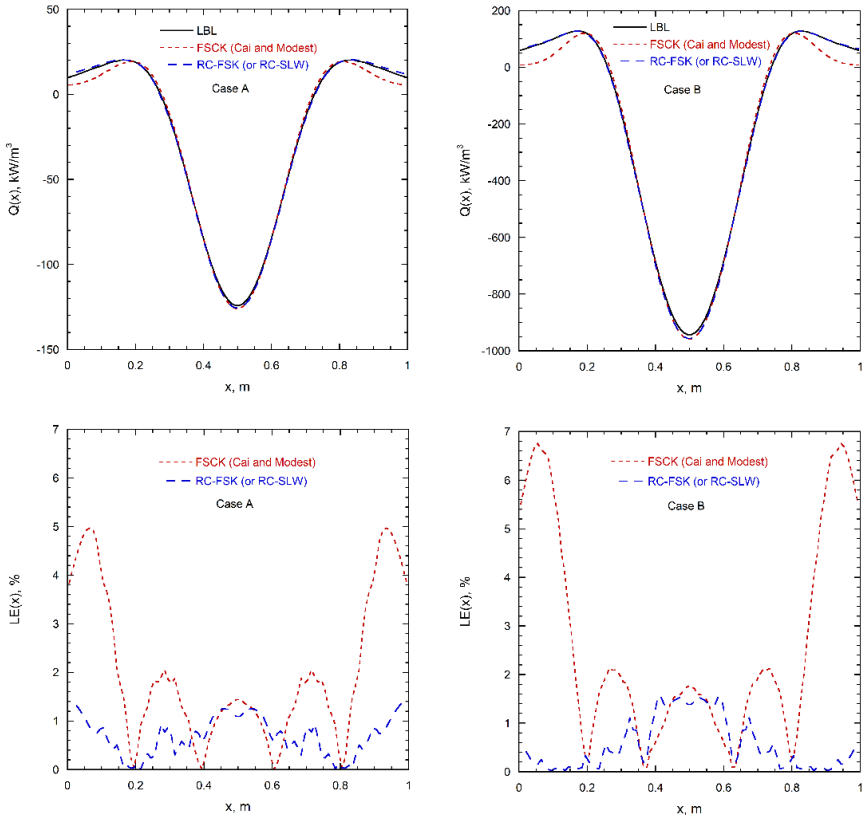

Figure 6. Predicted local divergence of the net radiative flux and local absolute error in the divergence predictions for Case A and Case B (adapted from Ref. [92]).

Finally, the primary differences between the two previous methods (FSCK and RC-FSK) are that i) the RC-FSK method does not require the arbitrary choice of a reference state to construct values of the absorption coefficient at local states inside the gas, and ii) grey gas weights are evaluated differently. Recent comparisons [98] between these two approaches have also shown that the FSCK scheme of Cai and Modest cannot be recommended in situations where absorption by gases is dominant, whereas both methods provide acceptable and similar accuracies in emission-dominant cases as encountered in most combustion applications. Consequently, in general, the RC-FSK method (or its SLW predecessor, the RC-SLW method) is now recommended for radiative heat transfer calculations [99].

4.1.7. *Summary*

Despite their apparent complexity, the full spectrum k-distribution methods are neither more complicated nor significantly more computationally demanding to use than the WSGG models. However, these full-spectrum k-distribution methods yield greater accuracy. Further, unlike the classical WSGG models, with available parameter databases k-distribution methods are applicable over a wide range of arbitrary gas species compositions, temperatures, and total pressures [70],[94]. A code built for RHT modeling using the WSGG model can be easily adapted to FSCK/RC-FSK methods, since the same RTE, Eq. (23), is solved in all these methods. The distribution functions required to generate the model parameters (local values of grey gas absorption coefficients and weights) can be found either in the form of correlations

([70]) or as look-up tables ([70],[100]-[104]). Look-up tables are more memory intensive than correlations, but are recommended because they offer greater simplicity (since the inversion of values in a look-up table is nearly effortless) and much improved accuracy.

Moreover, the FSCK models can be extended to mixtures of gaseous species of arbitrary mole fractions, or gas/non-grey absorbing particles mixtures, such as soot, without adding significant computational efforts when look-up tables are used [102],[103],[105]. It can be also extended to mixtures of gas and non-grey absorbing-scattering particles, such as coal, ash, char or droplets, also without adding significant computational efforts, as long as the scattering coefficient and phase function can be assumed to be grey [106],[107],[108],[109]. It should be pointed out that this latter approximation is generally valid even for extremely non-grey scatterers [109]. A compendium of the existing spectral gas radiative property approaches can be found, for instance, in Refs.[92],[93]. At the present time, the RC-FSK (RC-SLW) method is the most mature and robust full-spectrum techniques for radiative heat transfer calculations in gaseous mixtures. The FSCK method of Cai and Modest produces comparable predictive accuracy as the RC-FSK model in emission-dominated scenarios, but requires the arbitrary specification of a gas reference state and fails to provide the same accuracy in absorption-dominated situations.

4.2. Radiative properties of particles

4.2.1. General comments about particle-electromagnetic radiation interactions

As discussed in Section 4.1.1, gas emission and absorption spectra exhibit a distinct line structure because transitions of electrons in gas molecules are allowed only for certain quanta [6]. Unlike gases, a solid object emits and absorbs radiation continuously over the entire spectrum owing to the atomic orbitals overlap of a large number of atoms, leading to closely spaced atomic orbitals.

When incident light strikes an inhomogeneous medium, the incident light interacts with the medium and undergoes absorption and scattering. Since all media (except a vacuum) are formed by atoms and molecules, strictly speaking, they are inhomogeneous at the microscopic level, and scatter light. However, the importance of scattering is mainly dependent on the size parameter (the ratio of the scatterer perimeter to the incident light wavelength), in addition to the shape and optical properties of the scatterer. For thermal radiation in combustion systems where the peak temperatures are typically of the order of 2000 to 2500 K, the spectral range of interest falls between about 1 to 15 μm. Over this spectral range, light scattering by molecules and soot particles, which have characteristic diameters less than about 0.2 μm, can be neglected. However, light scattering by micron-sized particles, such as coal, char, and fly-ash, and droplets must be taken into account in modeling RHT in combustion systems.

The absorption and scattering properties of particles are determined by the optical property of the constituent material, i.e., the complex refractive index, the wavelength, and the particle shape, size, and number concentration. Although various particles encountered in combustion systems almost always have a complex shape, they are commonly treated as spheres based on the following three considerations. First, there is no analytical solution to the radiative properties of arbitrarily shaped particles and the numerical calculation is extremely time consuming. Second, for the simplest shape of spheres the Mie theory can be readily applied to

compute their absorption and scattering properties (absorption and scattering cross sections and the scattering phase function) at a given wavelength as long as their refractive index is known. Third, because a very large number of particles are randomly oriented in flames their average effect on RHT may be represented by homogeneous spherical particles. The radiative properties of particulates relevant to combustion applications have been extensively discussed in the review article of Viskanta and Mengüç [20] and the text book of Modest [6]. Only a brief and concise discussion of the radiative properties of solid particles in combustion applications is discussed below.

4.2.2. Radiative properties of soot

Soot is produced in the fuel-rich regions of a flame during incomplete combustion of hydrocarbon fuels or pulverized coal. As a result of diffusion limited cluster aggregation, soot particles appear as fractal-like aggregates formed by nearly spherical primary particles whose diameter, in general, falls in a relatively narrow range between 15 and 60 nm [110]. The aggregate size is often represented by the radius of gyration [111] and can span from few tens to few hundreds of nm. Because of their complex shape, the radiative properties of aggregated soot particles cannot be reasonably predicted by Mie theory using an equivalent sphere [111]. Fortunately, the fairly simple Rayleigh-Debyre-Gans approximation for fractal aggregates (RDG-FA) provides a convenient approach to evaluate the absorption and scattering cross sections of soot particles and scattering phase function with good accuracy [111]. Moreover, RDG-FA is very easy to implement due to its analytical form. Although the scattering properties of soot particles can be computed easily using RDG-FA, radiation scattering by sub-micron soot particles can be neglected since the size parameters at wavelengths relevant to thermal radiation in combustion are well within the Rayleigh scattering regime characterized by size parameters less than about 0.3. This theoretical conjecture has been verified numerically by Eymet et al. [112].

In RDG-FA, the absorption cross section of a soot aggregate is simply the summation of cross section of all the primary particles, which is evaluated using the Rayleigh expression,

$$C_a^{agg} = \sum_{I=1}^{N_p} C_a^{P_i} = \frac{\pi^2 E(m)}{\lambda} \sum_{i=1}^{N_p} d_i^3 \tag{26}$$

The quantity $E(m)$ is a function of the soot complex refractive index m given as:

$$E(m) = Im\left(\frac{m^2-1}{m^2+1}\right) \tag{27}$$

It is noticed that $E(m)$ is implicitly dependent on wavelength through the complex refractive index m. Eq. (26) indicates that the absorption cross section of soot particles is proportional to $E(m)$ and their volume, but inversely proportional to wavelength (or proportional to wavenumber, η). Therefore, the absortion cross section of soot particles decreases with increasing wavelength. The absorption coefficient of soot can be obtaiend by multiplying Eq. (26) with the primary particle number concentration, leading to the conclusion that the soot absorption coefficient is proportional to the soot volume fraction:

$$\kappa_S = \frac{6\pi E(m)}{\lambda} f_S = 6\pi E(m) f_S \eta \tag{28}$$

Although it is very straightforward to calculate the absorption coefficient of soot, in reality the absorption coefficient is subject to fairly large uncertainty through the uncertainty in soot refractive index m or its function $E(m)$. Based on extensive research on the morphology of microstructure of soot particles sampled from different flames fueled with different hydrocarbon fuels, it has been established in the combustion community that soot is not a very well defined material and displays differences in the C/H ratio, maturity, microstructure, and different levels of primary particle overlap and necking [113],[114]. Consequently, there are relatively large variations in the reported soot refractive index as discussed in the literature, e.g. by Liu et al. [115] and the references cited therein. It is also noticed that most of the studies of soot refractive index focused on the visible spectrum over which optically-based soot diagnostics is performed. Fewer efforts have been made to measure the soot refractive index in the infrared, which is relevant to RHT. The most commonly used soot refractive index for RHT modeling is the data obtained by Chang and Charalampopoulos [116] given as:

$$n = 1.811 + 0.1263 ln\lambda + 0.027 (ln\lambda)^2 + 0.0417 (ln\lambda)^3 \tag{29}$$

$$k = 0.5821 + 0.1213 ln\lambda + 0.2309 (ln\lambda)^2 - 0.01 (ln\lambda)^3 \tag{30}$$

which is applicable for $0.4 \leq \lambda \leq 30$ μm. It should be noticed that Eq. (28) is based on RDG-FA. Calculations of the radiative properties of soot fractal aggregates using numerically exact methods showed that the soot aggregate absorption cross section estimated by RDG-FA can be underestimated by up to 30% in the visible spectrum [111], though this deviation is expected to be smaller in the infrared. As a result of the spectral dependence of $E(m)$, the soot absorption coefficient given in Eq. (28) is only approximately proportional to wavenumber. This means that soot is a non-grey radiating specie and care should be taken to deal with mixtures containing soot and radiating gases. Different methods have been developed in the literature to deal with such mixtures within the context of SLW and FSCK models [109],[117]. Another challenge in predicting the contribution of soot to RHT in coupled combustion modeling lies in accurately predicting the distribution of soot volume fraction due to the relatively poor understanding of the soot formation mechanism [118],[119]. It is fortunate that the detailed knowledge of soot particle size is not required as far as RHT modeling is concerned.

4.2.3. Radiative properties of coal/char and fly-ash particles

In pulverized coal fired boilers and furnaces, RHT is strongly influenced by the presence of coal, char, and fly-ash particles [20]. In such combustion devices, coal particles are fed into the combustion chamber through burners. The coal particles are heated rapidly by convection and radiation to release volatiles and become char particles. The char particles oxidize, and remaining largely inorganic material becomes fly-ash particles with the burnout of carbon. Fly-ash particles, in general, play a more important role than coal and char particles in RHT, since the former are present in a large portion of the combustion chamber while the latter are only found in a relatively small volume in the near-burner region. As far as RHT is concerned, coal and char particles are commonly assumed to have the same radiative properties and same size. Because these particles are on the order of a few tens or hundreds of microns in size, their absorption and scattering behavior cannot be assumed to be in the Rayleigh regime. As argued in Section 4.2.1, it is reasonable to assume these particle are spherical and homogeneous on

average and consequently their radiative properties can be calculated by the Mie theory assuming that their size distribution and refractive index are known.

The radiative properties of char and ash particles, namely the spectral scattering and absorption cross sections and the scattering phase function, can be calculated by a proper Mie solution computer program, such as the Fortran program provided by Bohren and Huffman [120], as a function of the particle size parameter $\chi = \pi d/\lambda$ and the complex refractive index m. The available experimental data of the refractive index of coal/char particles have been reviewed by Viskanta and Mengüç [20]. The refractive index of char particles measured by Manickavasagam and Mengüç [121] remains a common choice [122],[106]. Experimental data for the refractive index of fly-ash are also relatively scarce and the majority were reported in the 80's and early 90's (see the references in Viskanta and Mengüç [20], Kez et al. [106] and Schiemann et al. [123]). The refractive index of fly-ash varies significantly with its chemical composition, which consist of varying amounts of oxides of silicon, aluminum, calcium and iron as well as ash, depending on the type and source of coal particles. The refractive index of fly-ash determined by Goodwin et al. [124] has often been used in numerical modeling of RHT in coal furnaces. The effect of fly-ash composition on RHT in coal-fired combustion systems has recently been investigated by Ateş et al. [125], who showed that the fly-ash composition and fly-ash refractive index model have a strong influence on the predicted heat flux and radiative source term.

The spectral scattering phase functions of char and fly-ash particles calculated by the Mie theory display rapid oscillations with the scattering angle, and this feature makes it impossible to directly use the Mie scattering phase function in solving RTE since it is computationally prohibitive to use angular discretization fine enough to resolve the Mie scattering phase function. It is a common practice to employ a simplified scattering phase function in modeling RHT in coal-fired combustion systems. The Henyey-Greenstein phase function and the transport approximation are the two most commonly used treatments to avoid the numerical difficulty of the Mie scattering phase function. The Henyey-Greenstein phase function is dependent only on the asymmetry factor g, which is calculated from the Mie theory, and is written as [6]:

$$\Phi(\theta) = \frac{1 - g^2}{[1 + g^2 - 2g\cos\theta]^{3/2}} \tag{31}$$

where θ is the scattering angle. It is noticed that the asymmetry factor g and hence the phase function also varies with wavelength. In the transport approximation, the scattering phase function is approximated by an isotropic component plus a δ-function factor written as [126]:

$$\Phi(\theta) = (1 - g) + 2g\delta(1 - \cos\theta) \tag{32}$$

The δ-dirac function component is introduced to represent the strongly forward scattering of char and fly ash particles. Like the Henyey-Greenstein phase function, the transport approximation phase function is also dependent only on the asymmetry factor g. A comparison of the Mie, Henyey-Greenstein, and transport approximation phase functions for 80 μm coal and 10 μm fly-ash particles at 1 μm wavelength can be found in Kez et al. [106].

4.2.4. Summary

The spectral radiative properties of soot, coal/char, and fly-ash particles can be readily calculated using the RDG-FA approximation and the Mie theory. The main uncertainty in the prediction of the absorption and scattering properties of these particles arises from the uncertainty in their refractive indices, which will propagate to the predicted radiative heat flux and source term. In addition to this challenge in the modeling of sooting and coal-fired flames, other difficuties arise when dealing with mixtures consisting of radiating gases and particles, which are unfortunately almost always the case in practical combustion systems. Due to the fairly mild variation of the spectral radiative properties of particles, they can be considered constant over narrow bands. Therefore, there is no difficulty in dealing with mixtures of gases and particles in narrow-band models. However, it is not tractable to apply narrow-band models for RHT modeling in engineering problems. The non-grey radiative properties of particles must be accounted for in accurate modeling of RHT in gas and particle mixtures when using wide-band or full-spectrum models. Although different strategies have been proposed to deal with RHT using global models in gas and particle mixtures, they lead to significantly higher computational time, or significantly larger look-up tables, or loss of accuracy.

5. Turbulence-radiation interaction (TRI)

5.1. Background

The Reynolds-averaged spectral RTE (without scattering by particles) and radiative source term in the energy equation can be written as follows [4]:

$$\boldsymbol{s}\cdot\boldsymbol{\nabla}\langle I_\eta\rangle = \langle\kappa_\eta I_{b\eta}\rangle - \langle\kappa_\eta I_\eta\rangle \tag{33}$$

$$\begin{aligned}\langle\frac{\partial \dot{q}''_{R,j}}{\partial x_j}\rangle &= 4\pi\langle\kappa_P(p_\alpha, f_S, T)I_b(T)\rangle - \int_0^\infty\left(\int_{4\pi}\langle\kappa_\eta(x_\alpha, p, f_S, T)I_\eta\rangle\, d\Omega\right)d\eta \\ &= 4\pi\langle\kappa_P I_b\rangle - \int_0^\infty\langle\kappa_\eta G_\eta\rangle\, d\eta\end{aligned} \tag{34}$$

Equations 33 and 34 can be reformulated to emphasize quantities related to the absorption and emission TRI, which result from the highly non-linear coupling between turbulent fluctuations in temperature, composition, and radiative intensity:

$$\langle\kappa_\eta(\phi)I_\eta\rangle = \kappa_\eta(\langle\phi\rangle)\langle I_\eta\rangle + \underbrace{\left[\langle\kappa_\eta(\phi)I_\eta\rangle - \kappa_\eta(\langle\phi\rangle)\langle I_\eta\rangle\right]}_{Absorption\ TRI} \tag{35a}$$

$$\langle\kappa_\eta(\phi)G_\eta\rangle = \kappa_\eta(\langle\phi\rangle)\langle G_\eta\rangle + \underbrace{\left[\langle\kappa_\eta(\phi)G_\eta\rangle - \kappa_\eta(\langle\phi\rangle)\langle G_\eta\rangle\right]}_{Absorption\ TRI} \tag{35b}$$

$$\langle\kappa_P(\phi)I_b(T)\rangle = \kappa_p(\langle\phi\rangle)I_b(\langle T\rangle) + \underbrace{\left[\langle\kappa_P(\phi)I_b(T)\rangle - \kappa_p(\langle\phi\rangle)I_b(\langle T\rangle)\right]}_{Emission\ TRI} \tag{36a}$$

$$\langle\kappa_\eta(\phi)I_{b\eta}(T)\rangle = \kappa_\eta(\langle\phi\rangle)I_{b\eta}(\langle T\rangle) + \underbrace{\left[\langle\kappa_\eta(\phi)I_{b\eta}(T)\rangle - \kappa_\eta(\langle\phi\rangle)I_{b\eta}(\langle T\rangle)\right]}_{Emission\ TRI} \tag{36b}$$

The influence of TRI on radiative fields, such as the radiative source term, radiative heat flux or radiant fraction, was evidenced in the early eighties (see [127] for example). In particular, Faeth and co-workers developed a methodology that consists of generating stochastic time

series of turbulent scalar fluctuations [128]-[135]. These instantaneous scalar values were used to solve the RTE along lines of sight and to determine the statistics of the instantaneous radiative intensity. Their approach was systematically applied to a vast amount of non-luminous and luminous flames. They proved that the radiative emissions are up to 50-300% higher when TRI is taken into account. These strong effects of TRI on radiative quantities were confirmed by numerical simulations covering a wide range of configurations, including atmospheric- and high-pressure lab-scale and large-scale non-luminous and luminous jet flames, lab-scale non-luminous and luminous pool fires and swirling oxy-fuel furnace [135]-[149].

On the other hand, radiation and TRI were also found to affect the flow field and flame structures. For non-luminous flames, it was found that they tend to reduce temperature gradients and smooth temperature fluctuations and, consequently, to reduce the turbulence levels [150],[144]. In sooting turbulent jet diffusion flames, recent Large Eddy Simulation (LES) of ethylene turbulent jet flames showed an opposite trend with larger temperature fluctuations when radiation is taken into account owing to the effects of soot dynamics [151]. Also, TRI needs to be included in many situations for accurate predictions of temperature [67] and kinetically-controlled processes such as the production of NO [142],[67] or soot [143],[152].

A vast amount of literature was devoted to TRI, including review papers [4][1],[153], as well as text book chapters [5],[6]. The following sections will focus on absorption and emission TRI in the framework of RANS. Section 2.4 will discuss TRI in LES.

5.2. Absorption TRI

The Reynolds-averaged absorption term can be developed as:

$$\langle \kappa_\eta I_\eta \rangle = \langle \kappa_\eta \rangle \langle I_\eta \rangle + \langle \kappa'_\eta I'_\eta \rangle \quad (37a)$$

$$\langle \kappa_\eta G_\eta \rangle = \langle \kappa_\eta \rangle \langle G_\eta \rangle + \langle \kappa'_\eta G'_\eta \rangle \quad (37b)$$

Absorption TRI is mainly caused by the non-linear coupling between fluctuations of the radiative intensity and fluctuations of the absorption coefficient (or incident radiation) ($\langle \kappa'_\eta I'_\eta \rangle$ or $\langle \kappa'_\eta G'_\eta \rangle$). The evaluation of this correlation is difficult because the fluctuations of the local intensity may be influenced by fluctuations that arise from spatial locations that can be anywhere in the medium. Modeling absorption TRI requires that one have a detailed knowledge of the instantaneous fields of temperature and composition, and that one solve the RTE over a significant amount of realizations of the flow. In decoupled fluid flow/radiation calculations, this can be done along line-of-sights by using the stochastic method proposed by Faeth and co-workers as described in Section 5.1 [141],[154]. In coupled fluid flow/radiation calculations, the particle photon Monte Carlo (PMC)/transported PDF method proposed by Modest, Haworth and co-workers takes advantage of the fact that transported PDF methods based on the Lagrangian Particles Method provide actual realizations of the flow [150],[143]. It is the only method reported to date capable of capturing exactly (without any approximation) absorption TRI. However, this scheme is time consuming and requires advanced RTE solvers such as the particle-based PMC method.

On the other hand, Kabashnikov and Myasnikova [155] and Song and Viskanta [156] suggested that the local fluctuations of the radiative intensity should be weakly correlated with the fluctuations of the local absorption coefficient as long as the turbulent eddies remains optically-thin (i.e., $\kappa_\eta L \ll 1$, L being the characteristic length scale of the turbulent eddies). This approximation, referred to as the Optically-Thin Fluctuation Approximation (OTFA) in the

literature, then simply consists of neglecting $\langle \kappa'_\eta I'_\eta \rangle$ (or $\langle \kappa'_\eta G'_\eta \rangle$) in Eqs. (37). The OTFA was found acceptable over a wide range of configurations, including lab-scale non-luminous jet flames [141], lab-scale luminous jet flames and pool fires [143], [157], large-scale luminous jet flames [143], [154] and high-pressure non-luminous jet flames [146]. These are welcome conclusions since the OTFA simplifies significantly the modeling of TRI and does not impose any restriction on the choice of the RTE solver.

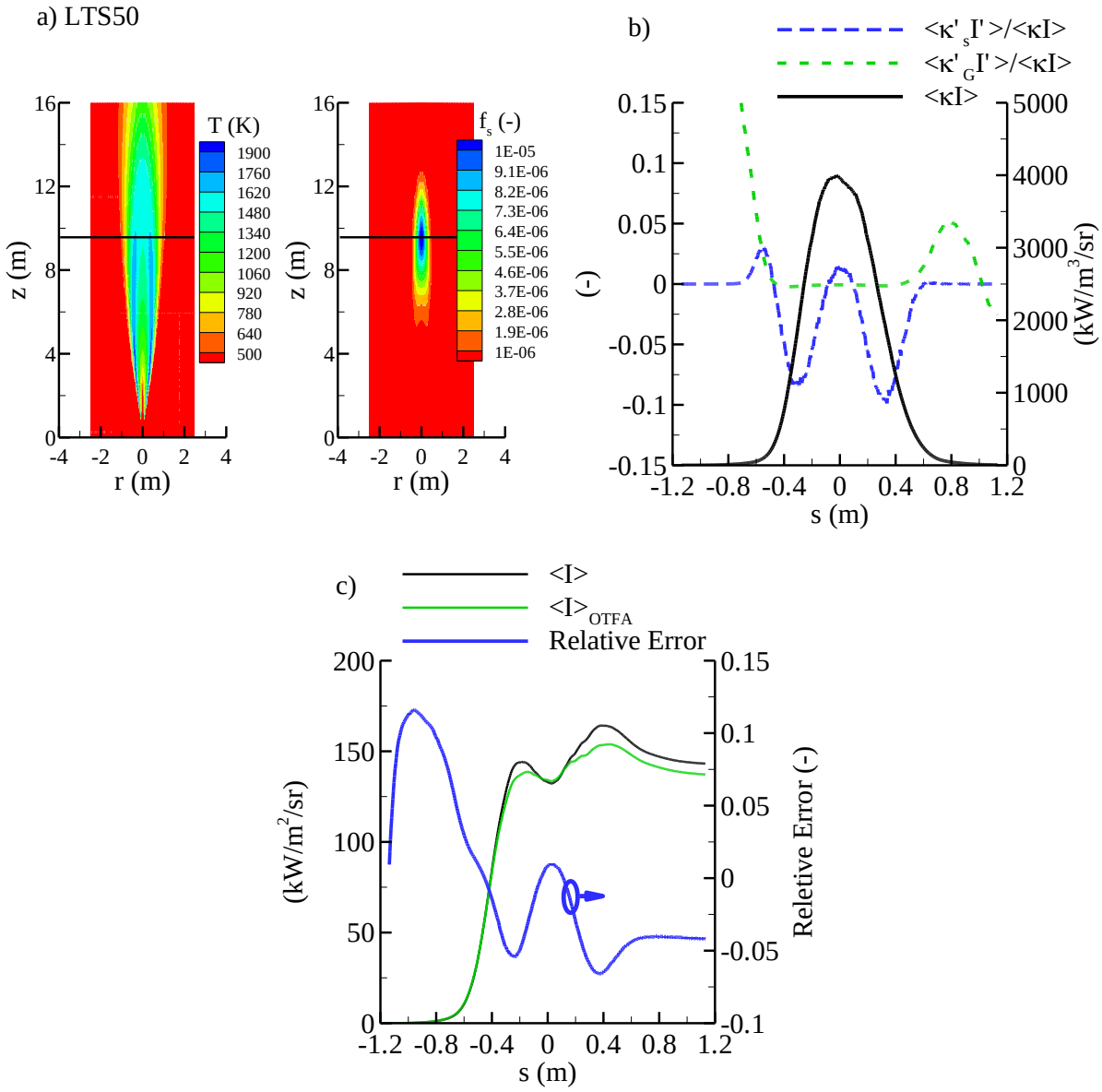

Figure 7. Effects of absorption TRI on radiative heat transfer along the line of sight crossing the region of maximum soot volume fraction in a large-scale ethylene flame: a) Fields of mean temperature and soot volume fraction. The horizontal line indicate the line of sight under consideration, b) Mean absorption term (right axis) and gas and soot absorption TRI (left axis) along the line of sight, c) effects of the OTFA on the prediction of the radiative intensity.

The effects of absorption TRI on radiative heat transfer along a diametric optical path crossing the region of maximum mean soot volume fraction in a large-scale turbulent jet ethylene/air

diffusion flame are illustrated in Fig. 7. This figure is adapted from Ref. [154]. This synthetic flame was generated by scaling the nozzle diameter of the lab-scale turbulent jet diffusion flame investigated by Lee et al. by a factor of 50 while maintaining the fuel injection velocity constant. The diametric path under consideration corresponds to the horizontal line shown in Figs. 7a. A stochastic space and time series model was used to generate instantaneous fields of soot volume fraction, temperature and mole fractions of radiating species along this line-of-sight. The fields were used to resolve the instantaneous RTE and compute the corresponding statistics. Figure 7b shows that gas absorption TRI is negligible in the region where mean absorption is important whereas soot absorption TRI contributes for less than 8% of mean absorption. This suggests that the OTFA can be applied. This is confirmed in Fig. 7c which shows that the radiative intensity computed by considering the OTFA is within 5% of that obtained with the complete model.

5.3. Emission TRI

Emission TRI depends only on local scalars such as temperature and composition, and its modeling is a closure problem similar to that encountered for chemical reaction rates owing to Turbulent-Chemistry Interaction. Therefore, its modeling is closely related to the turbulent combustion model used in the simulations. As such, emission TRI can be evaluated accurately by using one-time one-point joint PDF methods [135]-[146],[149],[150],[159] and transported PDF approaches provide an exact closure of this term in both non-sooting and sooting flames [135]-[137],[143],[146],[149],[150],[152]. Alternatively, moment-based closures of emission TRI, that consists in approximating the mean emission term by a Taylor series expansion and retaining only the lower-order moments, were also proposed [160]. Nevertheless, moment-based methods introduce empirical adjustable coefficients to match the experimental data. Fraga et al. revised recently this approach by fitting the unclosed high-order terms from Large Eddy Simulation (LES) in non-luminous pool fire configurations [161]. The updated model was found to provide a better agreement than the classical formulation. It should be pointed out that the use of moment-based closures was generally limited to simulations involving a combustion model that does not introduce a PDF such as the Eddy Dissipation Concept.

Emission TRI can be decomposed into the sum of three contributions, namely the spectral Planck function self-correlation (Term 1), the absorption coefficient self-correlation (Term 2) and the absorption coefficient-Planck function cross-correlation (Term 3):

$$\langle \kappa_\eta I_{b\eta} \rangle = \underbrace{\kappa_\eta I_{b\eta}}_{No\ TRI} + \underbrace{\kappa_\eta \left(\langle I_{b\eta} \rangle - I_{b\eta} \right)}_{Term\ 1} + \underbrace{\left(\langle \kappa_\eta \rangle \langle I_{b\eta} \rangle - \kappa_\eta \langle I_{b\eta} \rangle \right)}_{Term\ 2} + \underbrace{\left(\langle \kappa_\eta I_{b\eta} \rangle - \langle \kappa_\eta \rangle \langle I_{b\eta} \rangle \right)}_{Term\ 3} \tag{38a}$$

In Eq. (38a), quantities without brackets are evaluated from time-averaged variables, i.e., without accounting for TRIs. The sign of Term 1 can be obtained by a Taylor expansion of the spectral blackbody intensity. If terms of orders higher than 2 are neglected, Term 1 is approximated as:

$$\kappa_\eta \left(\langle I_{b\eta} \rangle - I_{b\eta} \right) \approx \kappa_\eta \left(\frac{\partial^2 I_{b\eta}}{\partial T^2} \right)_{T=\bar{T}} \frac{\langle T'^2 \rangle}{2} \tag{38b}$$

Equation (38b) shows that Term 1 is always positive and, as such, the spectral Planck function self-correlation tends to increase radiative emission. On the other hand, the signs of Terms 2 and 3 are less intuitive and may be different if gas or soot emission is considered.

In the case of gas emission, Terms 2 and 3 are also positive (see [137],[144] for example). Li and Modest used the FSCK method and a transported PDF method to investigate different TRI closures for the emission term (and also the absorption term) in SANDIA flame D and two synthetic flames generated from Flame D by scaling the fuel nozzle diameter by 2 and 4 times [137]. They found that the absorption coefficient–Planck function correlation (Term 1) is more important than the two other correlations. As a consequence, accurate determination of the temperature self-correlation alone appears insufficient in combustion gases. In addition, some calculations have shown that the increase in gas emission by TRI follows that of the optical-thickness [137],[149],[150].

In the case of soot emission, Term 2 in Eq. (38a) vanishes if soot is assumed to radiate in the Rayleigh regime, i.e., if the spectral soot absorption coefficient varies linearly with the soot volume fraction, $\kappa_{\eta,S} = C_\eta \eta f_S$ (see Eq. 28). An evaluation of Term 3 from a Taylor series expansion by neglecting components of orders higher than 2 shows that it scales with the correlation between soot volume fraction and temperature:

$$\langle \kappa_{\eta,S} I_{b\eta} \rangle - \langle \kappa_{\eta,S} \rangle \langle I_{b\eta} \rangle = \langle \kappa'_{\eta,S} I'_b \rangle \approx C_\eta \eta \left(\frac{\partial I_{b\eta}}{\partial T} \right)_{\bar{T}} \langle f'_S T' \rangle \tag{38c}$$

This correlation was observed to be negative in the region of strong soot emission in both experimental [162]-[165] and numerical [151],[152],[166],[166],[167] investigations of turbulent diffusion flames. Therefore, this term tends to reduce soot emission [152],[151],[166]. The effects of TRI on soot emission then results from a competition between temperature self-correlation effects that increase it and the negative correlation between the soot volume fraction and temperature that reduces it. Two mechanisms were found to be responsible for the negative correlation between soot volume fraction and temperature [166]. The first is directly related to the structure of the turbulent jet flame through complex interaction between mixture fraction and soot properties in the oxidation region and, as such, is independent of the fuel, whereas the second is due to the soot emission process itself. Finally, it should be pointed out that, in RANS simulations, only TRI emission models based on transported PDF approaches, which provide a direct access to the joint PDF of gas-phase and soot-phase properties, were reported to date to account for the effects of this negative correlation.

TRI effects on flame radiative loss in sooting turbulent flames are then governed by competing mechanisms [149],[168]. Enhancement mechanisms are due to gas emission TRI and temperature self-correlation effects on soot emission whereas the reduction mechanism is caused by the negative correlation between soot volume fraction and temperature. Simulations results demonstrated that the latter becomes increasingly important as the soot volume fraction increases and may be dominant locally and even globally in the case of highly sooting flames [168],[149].

5.4. TRI in LES

The local spatially filtered value of a physical quantity Q, $\bar{Q}$, is defined as [34]:

$$\bar{Q}(x,t) = \int Q(y,t)G(|x-y|)dy \tag{39}$$

where integration is performed over the entire flow domain. G is a low-pass spatial filter function with a characteristic filter width Δ. The instantaneous value of Q in a turbulent flow can be decomposed into a filtered (or resolved) component, $\bar{Q}$, and a subfilter (or residual) fluctuation around the filtered component, Q'':

$$Q(x,t) = \bar{Q}(x,t) + Q''(x,t) \tag{40}$$

The filtered RTE and divergence of the radiative flux are obtained by applying the filtering operation to Eqs. 2 and 3:

$$\boldsymbol{s}\cdot\boldsymbol{\nabla}\bar{I}_\eta = \overline{\kappa_\eta I_{b\eta}} - \overline{\kappa_\eta I_\eta} \tag{41}$$

$$\frac{\overline{\partial \dot{q}''_{R,J}}}{\partial x_J} = 4\pi\overline{\kappa_P I_b} - \int_0^\infty \overline{\kappa_\eta G_\eta}\, d\eta \tag{42}$$

The filtered absorption, $\overline{\kappa_\eta I_\eta}$ (or $\overline{\kappa_\eta G_\eta}$), and emission, $\overline{\kappa_P I_b}$, terms are decomposed into a sum of resolved-scale and subgrid-scale (SGS) contributions.

$$\overline{\kappa_\eta G_\eta} = \underbrace{\kappa_\eta(\bar{\phi})\overline{G_\eta}}_{Resolved} + \underbrace{\left[\overline{\kappa_\eta G_\eta} - \kappa_\eta(\bar{\phi})\overline{G_\eta}\right]}_{SGS} \tag{43}$$

$$\overline{\kappa_P I_b} = \underbrace{\kappa_P(\bar{\phi})I_b(\bar{T})}_{Resolved} + \underbrace{\left[\overline{\kappa_P I_b} - \kappa_P(\bar{\phi})I_b(\bar{T})\right]}_{SGS} \tag{44}$$

The resolved and SGS fluctuations in temperature and composition related to absorption and emission TRI can then be calculated as:

$$\langle\kappa_\eta G_\eta\rangle \approx \underbrace{\kappa_\eta(\langle\bar{\phi}\rangle)\langle\overline{G_\eta}\rangle}_{NoTRI} + \underbrace{\underbrace{\left[\langle\kappa_\eta(\bar{\phi})\overline{G_\eta}\rangle - \kappa_\eta(\langle\bar{\phi}\rangle)\langle\overline{G_\eta}\rangle\right]}_{Resolved\ absorption\ TRI} + \underbrace{\left[\langle\overline{\kappa_\eta G_\eta} - \kappa_\eta(\bar{\phi})\overline{G_\eta}\rangle\right]}_{SGS\ absorption\ TRI}}_{Absorption\ TRI} \tag{45}$$

$$\langle\kappa_P I_b\rangle \approx \underbrace{\kappa_P(\langle\bar{\phi}\rangle)I_b(\langle\bar{T}\rangle)}_{NoTRI} + \underbrace{\underbrace{\left[\langle\kappa_P(\bar{\phi})I_b(\bar{T})\rangle - \kappa_P(\langle\bar{\phi}\rangle)I_b(\langle\bar{T}\rangle)\right]}_{Resolved\ Emission\ TRI} + \underbrace{\left[\langle\overline{\kappa_P I_b} - \kappa_P(\bar{\phi})I_b(\bar{T})\rangle\right]}_{SGS\ Emission\ TRI}}_{Emission\ TRI} \tag{46}$$

It should be pointed out that only the SGS TRI requires modeling. On the other hand, the relative contributions of resolved and SGS TRI depend on the filter size: SGS TRI diminishes with decreasing filter width (mesh size) whereas, in an opposite way, the resolved TRI increases with larger mesh sizes [169],[170]. This raises questions of the importance of SGS TRI and its proper modeling.

Several works demonstrated that SGS absorption TRI can be neglected [169],[170],[171]. The work of Gupta et al. [171] deserves particular attention since their modeling involved an advanced transported filtered density function (FDF)/photon Monte Carlo (PMC) method/LBL

radiation model which captures SGS absorption TRI in coupled calculations. This radiation model was applied to the LES of non-sooting and sooting flames of different optical thicknesses derived from the Sandia flame D and about 84% of the turbulence kinetic energy was resolved in their simulations. In these situations, they found that SGS absorption TRI can be disregarded.

As for emission TRI, the modeling of SFS emission TRI is strongly dependent on the turbulent combustion model used in the simulations. An accurate way to model SFS emission TRI is to consider FDF approaches [171],[172],[173]. On the other hand, several studies relative to LES of fire related configurations have extended to LES the moment-based closure proposed by Snegirev for RANS [174],[175],[176]. The importance of SGS emission TRI is strongly dependent on the filter size. From a practical perspective, recent works showed that, for a filter size typical of engineering applications, the effects of SGS fluctuations on the filtered emission term have to be modeled [170] and can even exceed those of resolved-scale fluctuations [171]. However, there is no consensus about this issue, and other works suggest that the error introduced by neglecting SGS emission TRI is marginal [172],[173].

6. Importance of radiation in small-scale flames

In this section, we will restrict our discussion of the importance of RHT to small-scale and certain fundamental flame phenomena. The focus of literature discussion is primarily on numerical and experimental studies. The present discussion of the importance of RHT in combustion is by no means comprehensive, since RHT affects essentially all aspects of flame and combustion and has been investigated using theoretical approach in addition to experiments and numerical simulation.

6.1. Importance of RHT in premixed flames

6.1.1. Flammability limits

We start the discussion of the importance of radiation heat loss to the presence of a fundamental flammability limit, which is defined as a critical fuel concentration in air below which the mixture is non-flammable. Clearly, it refers to the lean flammability limit. The rich flammability limit can be defined similarly as a critical fuel concentration about which the mixture is non-flammable. Although the mechanism responsible for the presence of the fundamental limit was debated for quite a long time, it has been accepted that the inherent radiation heat loss is responsible for the presence of the fundamental limits. This conclusion was reached after studies conducted over the last several decades by various researchers, such as Spalding [177], Berlad and Yang [178], Gerstein and Stine [179], Ronney [180], Lakshmisha et al. [181], and Ju et al. [182],[183].

In early studies of the extinction and flammability limit of freely-propagating premixed flames, the effect of radiation heat loss was generally accounted for in a highly approximate manner. Lakshmisha et al. [181] were among the first researchers to employ fairly detailed combustion chemistry and the OTA of RHT to predict extinction and the lean flammability limit of CH_4/air mixtures. They used the curve-fitted Planck absorption coefficients of CO_2 and H_2O of Hubbard and Tien [184] in their numerical simulation. Their study clearly demonstrated that radiation heat loss from the flame is responsible for the flame extinction when the lean flammability limit is approached. In addition, their predicted lean flammability limit of CH_4/air mixture is in good agreement with available measurements. As pointed out by Williams [185], the fundamental

limit caused gas radiation heat loss should be independent of the experimental apparatus as long as the apparatus is sufficiently large to minimize wall heat conduction loss.

It has been established that the presence of flammability limits of a fuel mixture is determined by the inherent radiation heat loss. Although it is generally true to state that the lean flammability limit is fundamental (independent of experimental apparatus) since the radiation absorption effect of fuel/air mixtures is very weak, this is no longer true when the mixtures are strongly radiatively absorbing by seeding with inert and radiating particles as pointed out by Ronney [180]. In this case the fresh mixture is preheated by absorbing radiative energy emitted by the burnt hot products and the degree of preheating depends on the type and concentration of absorbing particles [186] or absorbing gases, such as CO_2 [187]. A similar concern may arise in rich fuel/air mixtures due to the potential apparatus dependence of the radiation absorption of the fresh mixture containing high concentration of hydrocarbon. However, it seems that there have been no studies addressing the potential importance of radiation absorption in rich fuel/air mixtures.

6.1.2. Radiation-induced extinction of counterflow premixed flame

In burner-stabilized counterflow premixed flames, radiation heat loss from the hot reaction zone not only alters the temperature distribution, but also can cause flame extinction when the stretch rate is sufficiently small. Radiation-induced premixed flame extinction has been experimentally observed under microgravity by Maruta et al. [188]. Since radiation-induced flame extinction occurs at a sufficiently low stretch rate, this phenomenon cannot be observed on earth due to the buoyancy-induced convection, which acts as disturbance or stretch to the flames. Maruta et al. [188] experimentally investigated a counterflow twin-premixed flame. In this configuration, identical mixtures are issued from two opposing identical cylindrical nozzles to establish two premixed flames, which are identical and located symmetrically about the stagnation plane. They found that there exists two stagnation velocity gradients at extinction for a flammable mixture: a higher value represents stretch-induced extinction at high stretch and a lower value denotes the radiation-induced extinction at low stretch. At a critical equivalence ratio there is only one extinction velocity gradient and this critical equivalence ratio corresponds to the lean flammability limit of counterflow premixed CH_4/air flame, which is actually different from the lean flammability limit of freely-propagating CH_4/air premixed flame as shown by Ju et al. [182].

The extinction phenomenon of counterflow twin premixed flame of CH_4/air mixtures was numerically modeled by Guo et al. [189], who employed the CHEMKIN code along with a detailed C1 chemistry model and the OTA for radiation heat loss. The Planck mean absorption coefficients of CO_2 and H_2O as a function of temperature were calculated from the work of Tien [190]. The numerical results of Guo et al. [189] reproduced the experimental finding of Maruta et al. [188], though the predicted lean flammability limit of counterflow premixed CH_4 flame is lower than the measurement (0.42 vs. 0.469). The potential causes of this discrepancy have been discussed by Maruta et al. [188]. Guo et al. showed that the ratio of radiation heat loss from the flame to the total heat release of the flame increases rapidly to more than 20% at stretch rates close to radiation-induced extinction [189]. Moreover the twin flames are apart from each other at intermediate stretch rates and move very close to each other at both high stretch and low stretch. If radiation heat loss is neglected, the peak flame temperature decreases very slowly with decreasing the stretch rate due to the Lewis number effect and flame extinction will not occur, confirming that radiation heat loss is the mechanism of flame extinction at low stretch.

Ju et al. [183] conducted a comprehensive numerical study of the combined effect of radiation heat loss and stretch in the counterflow twin-premixed flame configuration to understand the relationship between the stretched counterflow and planar freely-propagation premixed flames. They showed that the combined effects of RHT and stretch results in very interesting phenomena in counterflow premixed flame that otherwise do not occur in planar freely-propagating premixed flames. A counterflow premixed CH_4/air flame can be reduced to a planar freely-propagating flame only when the equivalence ratio is above a critical value under the combined effects of radiation heat loss and the Lewis number. The combined effects of radiation heat loss and Lewis number on the bifurcation and extinction of counterflow twin-premixed $CH_4/(O_2\text{-}N_2\text{-He})$ flames was numerically investigated by Ju et al. [191]. The Planck mean absorption coefficients of CO, CO_2, and H_2O were calculated from the statistical narrow-band (SNB) model using the dataset of Soufiani and Taine [192]. They showed that multiple stable flame states at a given equivalence ratio can exist by varying the Lewis number through changing the ratio of N_2 and He in the mixture. RHT plays a vital role in the occurrence of the complex flame bifurcation.

In lean premixed CH_4/air flames, radiation absorption is likely unimportant and the use of OTA is largely justified. However, the importance of radiation absorption on the extinction and flammability limit of counterflow-premixed flames may not be neglected when the fresh mixture contains a significant amount of absorbing species, such as water vapor or CO_2. The importance of radiation absorption in premixed CH_4 flames with CO_2 addition has been investigated in several studies. Guo et al. [193] numerically modeled the counterflow premixed flames of CH_4/air, $CH_4/(\text{air-}CO_2)$, and $CH_4/(O_2\text{-}CO_2)$ using the CHEMKIN code and the C1 chemistry. The $CH_4/(\text{air-}CO_2)$ and $CH_4/(O_2\text{-}CO_2)$ mixtures were obtained by adding a certain amount of CO_2 to air and by replacing N_2 in air with CO_2, respectively. Instead using OTA for RHT, they took into account the effect of radiation reabsorption by solving the RTE using DOM. However, they used the grey-gas model and the Planck mean absorption coefficients of Tien [190]. Their results showed that the effect of radiation absorption is very minor on the flame temperature and radiation extinction stretch rate of lean CH_4/air flames, which is somewhat expected due to the low concentrations of CO_2 and H_2O. However, radiation absorption becomes important in the $CH_4/(90\%\text{air-}10\%CO_2)$ and $CH_4/(O_2\text{-}CO_2)$ flames due to the higher concentration of CO_2 in the mixture. Radiation absorption was found to mainly affect the radiation extinction stretch rate, but has a small influence on the stretch extinction limit. Although radiation absorption is important in counterflow premixed $CH_4/(O_2\text{-}CO_2)$ flames, the radiation-induced extinction stretch rate is significantly higher than that of CH_4/air flames due to enhanced radiation loss and reduced flame temperature as a result of the higher heat capacity of CO_2 than N_2.

The importance of radiation absorption to the propagation and extinction of planar freely-propagating premixed $CH_4/(0.21O_2+(0.79\text{-}\gamma)N_2+\gamma CO_2)$ flames was investigated by Ju et al. [182]. RHT was modeled using the SNB model with and without the absorption term. The presence of a large amount of CO_2 in the fresh mixture ($\gamma = 0.3$) absorbs the thermal radiation emitted from the hot products to preheat the mixture, which cannot be captured if RHT is neglected or radiation absorption is not considered (OTA). The three treatments of RHT, namely adiabatic, with absorption, and OTA, lead to different laminar burning velocity of 7.9, 12.7, and 5.9 cm/s, respectively. Therefore, the mixture preheating due to radiation absorption strongly enhances the laminar burning velocity. Although radiation absorption has a fairly small effect on the lean flammability limit of CH_4/air flames, equivalence ratio of 0.468 vs. 0.488, it has a very strong effect for the flames of $\gamma = 0.3$. For near-limit mixtures neglect of radiation

absorption, i.e., using OTA, failed to predict the flame propagation when the amount of CO_2 in the mixture is above a certain level, further demonstrating the importance of considering radiation absorption in absorbing premixed flames.

The importance of radiation absorption in spherically-propagating premixed flames at elevated pressures has been investigated by Chen et al. [187] by solving the RTE using the DOM and the SNBCK model. Overall, their findings are qualitatively similar to those of Ju et al. [182]. They also found that increasing pressure enhanced the importance of RHT and radiation absorption and it is important to consider the spectral dependence of radiating gases. In addition to its effects on flammability limit, propagation, and extinction mentioned above, RHT can also induce flame instability as shown in the study of Ju et al. [194].

6.2. Radiation-induced extinction of diffusion flames

Radiation-induced extinction is also observed in diffusion flames. It is opposite to the kinetic extinction mode [195],[196], which occurs when the mixing time (or residence time) becomes significantly lower than the characteristic time for the chemical reactions (low Damkhöler number, Da). The radiation-induced extinction (or radiative quenching) exists only in the presence of radiative heat loss, and occurs at long residence times (large Da). The energy loss through radiation causes a decrease in flame temperature, leading to a reduction of the reaction rates. Quenching takes place when excess heat loss significantly lowers the reaction rate such that the flame can no longer sustain itself [197]. The radiative quenching has been less studied than the kinetic quenching because it is more difficult to observe on earth as the intrusion of buoyant force accelerates the flow and reduces the residence times. The microgravity environment offers unique conditions to investigate radiative flame quenching due to the long residence times encountered.

The potential importance of radiation heat loss to flame extinction was perhaps first noticed by Bonne in 1971 [197]. He simulated microgravity flames in laboratory by generating “thick” and “flat” laminar diffusion flames and reached the following two important conclusions based on experiments and numerical modeling: (i) radiative heat transfer cools the flames significantly to the point that the visible soot luminosity disappears, and (ii) very sooty diffusion flames will reach radiative extinction before non-sooty flames. Extinction of a condensed fuel diffusion flame in the stagnation-point region of a forced flow can occur at a low stretch rate due to the radiation heat loss from the fuel surface [198]. Radiation-induced flame extinction at low stretch in counterflow diffusion flame due to gas-phase radiation loss has been suggested in the numerical studies of Platt and T’ien [199] and Liu and Rogg [200]. Maruta et al. [201] conducted a combined experimental and numerical study to investigate the extinction behaviour of a counterflow N_2-diluted CH_4/air diffusion flame at low stretch. Experiments were conducted at microgravity to avoid the buoyancy induced convection. Numerical modeling was conducted using the same methods employed by Guo et al. [189]. Both the measurements and modeling indicate that the extinction stagnation-point gradient at a given fuel concentration is double valued. The velocity gradient at the upper and lower branches corresponds to, respectively, the stretch extinction limit and the radiation extinction limit. The mechanism of radiation-induced extinction in counterflow diffusion flame at low stretch is attributed to the increased radiant fraction (the ratio of radiation heat loss from the flame to the total heat release) because of the broadened reaction zone and increased residence time caused by the decrease in the stretch rate. Nevertheless, radiation heat loss from the flame causes extinction of both counterflow premixed and counterflow diffusion flame at a sufficiently low stretch.

Radiative extinction was also intensively investigated in burner-stabilized spherical diffusion flames [202]-[210]. The corresponding experiments are generally performed in micro-gravity to maintain spherical symmetry. Mills and Matalon [202] and Wang and Chao [203] have identified the kinetic and radiative extinction limits of steady diffusion flames. Propagation and radiative extinction of transient flames were also studied experimentally and numerically by Tse et al. [204], Santa et al. [205],[206] and Tang et al. [208],[209], where they observed that the extinction behaviour is different from steady flames.

Radiative quenching was also observed at the flame trailing edge of microgravity boundary layer diffusion flames in microgravity. This configuration, where a flame sets over a fuel plate supported by a low oxidizer flow blowing parallel to this surface, is a canonical scenario for the fire safety purpose since it is associated with flame spread over solid and liquid fuel flat-surfaces. The mechanisms leading the flame quenching at the flame trailing edge are intimately related to enhancement of residence times that favors the production of soot and resulting radiative heat transfer. In particular, this extinction process controls the flame length that was observed to increase with the oxidizer velocity [211]-[214]. This behavior is opposite to that expected when complete combustion occurs [214],[215]. Contreras et al. [15] confirmed this quenching process by modeling microgravity ethylene/air laminar boundary layer diffusion flames with a detailed gas-phase reaction mechanism and a PAH-based soot production model. RHT was calculated using the DOM coupled to a wide-band correlated-*k* model. They showed that the combustion efficiency is significantly lower than unity and is reduced as the flow residence time increases.

6.3. The importance of RHT in 2D laminar diffusion flames

While the primary focus of this review is the impact of radiation transfer in turbulent flames, its impact on laminar flames warrants some coverage as well. RHT also plays important role in laminar coflow diffusion flames, especially in microgravity. It has been shown by Liu et al. [216] that RHT in laminar coflow C_2H_4/air diffusion flames prolongs the flame height and lowers the peak flame temperature, though it does not change significantly the peak soot volume fraction. RHT and radiation absorption in a laminar coflow C_2H_4/air diffusion flame established with a 10.9 mm inner diameter fuel tube at atmospheric pressure were shown to be significantly more important at microgravity than at normal earth gravity [217]. Using the same coflow diffusion flame burner, Kong and Liu [218] showed that the flame centerline temperatures decrease significantly due to radiation heat loss at microgravity in a laminar coflow CH_4/air diffusion flame when the coflow air stream velocity is very low. Under these conditions, the predicted soot volume fractions are very low. They argued that flame extinction, or at least partial flame extinction along the centerline region, may occur due to excessive radiation heat loss from the flame if the coflow air stream velocity is further reduced. However, this conjecture needs to be validated by experiments in microgravity. Demarco et al. also investigated RHT in axisymmetric laminar coflow diffusion flames [11] by using the Steady Laminar Flamelet (SLF) model, a semi-empirical two-equation acetylene/benzene based soot model and the Statistical Narrow Band Correlated *k* model coupled to the Finite Volume Method. They simulated twenty-four C_1–C_3 hydrocarbon–air flames, consisting of normal and inverse (IDF) diffusion flames at both normal gravity and microgravity, predicting a reasonable agreement with available experimental data in terms of velocity, temperature, soot volume fraction and radiative losses. Their conclusions were in line with those drawn by Liu and co-workers, i.e., accounting for thermal radiation is critical for accurate predictions of temperatures and soot concentrations and its influence is increasingly significant from inverse to normal diffusion flames and much greater as gravity is reduced. They quantified also the relative contributions

of gas and soot, showing that both contributions are significant in all cases, with the exception of the 1g IDFs investigated where soot radiation can be ignored.

The role of RHT on the opposed flow spreading behavior of non-buoyant diffusion flames over thin electrical wires coated by low-density polyethylene was investigated recently through experiments, theory and numerical computations [12],[219]. Measurements were performed in parabolic flights and flame spread rate, pyrolysis rate, stand-off distance, soot volume fraction, and soot temperature were experimentally determined based on optical diagnostics that capture the flame spread in parabolic flights. In particular, a broadband modulated absorption emission technique was specifically developed to measure soot volume fraction and soot temperature [220]. The theoretical [219] and numerical [12] studies considered a flame spreading at atmospheric pressure in an O_2 /N_2 oxidizer composed of 19% oxygen in volume and a flow velocity of 200 mm/s. The numerical model was based on the solution of transport equations in an axisymmetric flame-fixed coordinate system in conjunction with a simple degradation model for the Low Density PolyEthylene (LDPE) and a radiation model combining the Full-Spectrum Correlated-*k* method with the Finite Volume Method. Comparisons between model predictions and experimental data in terms of flame structure and soot volume fraction were found in agreement with experimental data. These studies showed that radiation contributes negatively to the surface heat balance along the LDPE molten surface and the coating ahead of the molten front, suggesting that the convective heat transfer from the flame is the main contribution to sustain the pyrolysis process and the flame spread. In addition, soot radiation was found to dominate the radiative heat transfer in this flame, contributing about two-thirds of the total radiation [12].

7. Recent simulations with advanced radiation models

This section presents representative simulations of turbulent flames or industrial combustion systems by using advanced radiation sub-models. It includes works devoted to simulations of turbulent flames, high-pressure internal combustion engines, combustors and coal combustion. It is limited to works published since 2016 since studies published prior to this were exhaustively reviewed in the textbooks by Modest and Haworth [5] but also by Coelho [221]. This latter textbook addresses laboratory combustion chambers and industrial applications, including gas turbines, boilers and furnaces.

7.1. Turbulent flames

Rodrigues et al. [151] performed LES of the turbulent jet ethylene/air investigated experimentally at Sandia [222]. They combined the non-adiabatic flamelet progress variable model proposed by Ihme and Pitsch [223] with a detailed sectional PAH-based soot production model. SGS turbulence/chemistry and turbulence/soot production interactions were modeled with the presumed FDF approaches reported in Ref. [224]. Radiation was modeled using a MC method as RTE solver and the NBCK as gas radiative property model. SGS TRI was neglected. Model predictions were in satisfactory agreement with the experimental data for both gas-phase (mean temperature and species, rms of temperature and species) and soot-phase quantities (soot intermittency, soot volume fraction). In addition, computed radiative intensity were also found in good accordance with measurements. A comprehensive analysis of the radiative structure of the flame was reported. In particular, as discussed in the Section 6 devoted to TRI, they observed opposite effects of turbulence-radiation interactions for the gaseous and the soot contributions. The increase in mean emitted power for the gaseous phase was attributed to temperature fluctuations whereas a decrease of the soot-phase contribution was related to the negative temperature-soot volume fraction correlation.

Wu et al. [225] reported detailed modeling of the small-scale heptane pool fire (diameter 7.1 cm) investigated experimentally by Klassen and Gore [226]. Chemistry and soot production were modeled by a 33-species skeletal mechanism and a two-equation acetylene-based model, respectively. Turbulence was fully resolved by the grid. Radiation was modeled using the LBL PMC developed by Modest and co-workers [33], and the contributions of CO_2, H_2O, CO, CH_4, C_2H_4 and soot were taken into account. The model reproduced correctly the flame structure as well as the measured radiative fluxes and line-of-sight spectral distribution of the emissive power. They showed that soot radiation is largely optically thin whereas a more significant part of gas emission is re-absorbed within the flame. This latter conclusion is in line with that drawn in other numerical studies of lab-scale turbulent diffusion flames [143],[151],[168].

RANS simulations of oxygen-enriched turbulent jet flames fueled by propane and methane/ethylene blends were reported in Ref. [227]. Turbulence-chemistry interaction, turbulence-soot production-interaction and emission TRI were modeled by a hybrid flamelet/transported PDF approach whereas absorption TRI was neglected assuming the OTFA. Soot production was modeled with a two-equation acetylene/benzene model. The spectral dependence of the absorption coefficient of the radiating gases and soot was computed by a wide-band correlated-*k* (WBCK) method and the Finite Volume Method was used as RTE solver. Model predictions in terms of soot volume fraction, radiant heat flux distribution along the wall of the combustion chamber, and radiant fraction agreed reasonably well with the experimental data of [19]. In addition, the model was able to predict the non-monotonic evolution of the soot production with the oxygen index (volume fraction of oxygen the oxidizer), increasing sharply when the oxygen-index is enhanced from 21% to about 40% and then being significantly reduced as the oxygen index is further increased.

7.2. High pressure internal combustion engines

The design of high-pressure internal combustion engines is more and more challenging due to increasingly stringent regulation on fuel consumption and pollutant emissions such as soot and NO_x. Several works focused on the numerical modeling of the ECN Spray A. This refers to a transient high-pressure turbulent n-dodecane spray flame operating under conditions that are relevant for compression-ignition piston engines (60 bars) [228]-[231]. Bolla et al. [228] performed RANS simulations and compared two combustion models, namely a transported PDF model and a simpler well-mixed (WM) model that neglects turbulence-chemistry interaction and TRI. A grey RTE formulated using the Planck-mean absorption coefficients of the radiating species (CO_2, H_2O and soot) was solved by the DOM. They showed that radiation and TRI effects are small in this configuration. These conclusions were confirmed by Fernandez et al. [229] with a more advanced radiation model involving the LBL/PMC method coupled to a transported PDF approach to model TRI. The contribution of CO_2, H_2O, CO and soot were taken into account. Mukut and Roy [230] extended this radiation model by including the radiative contribution of the spray phase using the formulation developed by Roy et al. [231]. They showed that the effect of spray and gas phase radiation on soot is minimal in the ECN Spray A combustion chamber and gas-phase radiation has a greater influence on NO formation than the spray-phase radiation. Paul et al. [232] used the same model as Fernandez et al. [229] to perform an in-depth investigation of radiative heat transfer for a heavy-duty diesel truck engine over a range of operating conditions. They showed that redistribution energy is dominated by CO_2 and H_2O is mainly responsible for the radiative heat loss. These findings were used in another work to propose a computationally efficient stepwise-grey model that

provides predictions within 10% deviations from the results of accurate spectral radiation models [233].

7.3. Combustors

LES of practical combustors were reported in Refs. [234],[235]. A particular attention was put on wall heat conduction and RHT to predict the wall temperature of the combustion chamber. Berger et al. [234] conducted LES of a helicopter combustor. Radiation was modeled by coupling the DOM to the Full Spectrum based on the SNBCK model [236] for the radiative properties of CO_2, H_2O and CO. Their simulations showed that LES can be coupled with wall conduction at an acceptable computational cost in industrial configurations and provided predictions in quantitative agreement with thermocolor experimental data. Koren et al. [235] reported LES of a confined premixed swirling flame operating under atmospheric pressure as investigated experimentally in Refs. [237],[238]. The model considered a non-adiabatic Filtered Tabulated Chemistry for LES model [238] and a self-adaptive coupling procedure for conjugate heat transfer [239]. The RTE was solved by a Monte Carlo method and the NBCK was used to compute the radiative properties of CO_2 and H_2O. The experimental wall temperature was well reproduced by the numerical simulations.

7.4. Coal combustion

Oxy-coal combustion is an important technology for carbon capture in coal-fired power plants. In such conditions, the concentration of CO_2 is elevated and the heat transfer can be dominated by RHT, which becomes in turn a critical component for the boiler design. The importance of considering non-grey gas radiation model was established [240],[241] as well as the impact of the particle distribution on the prediction of radiative heat transfer [242]. Wu et al. [240] carried out RANS simulations of a lab-scale pulverized coal flame using an Eulerian-Lagrangian description of the multiphase flow and a detailed chemistry coupled to a PaSR model. A Monte Carlo ray tracing model was considered as RTE solver. The non-grey radiative property of the gas (CO_2, H_2O and CO) and solid phases were modeled with a LBL database and a size dependent non-grey correlation, respectively. A parametric study showed that considering non-grey gas radiation affects significantly emission and absorption source terms whereas non-grey solid-phase radiation results in less significant differences. Seidel et al. [243] performed RANS simulations of non-swirling oxy-coal flames to assess the capability of Eulerian-Eulerian and Eulerian-Lagrangian descriptions of the multiphase flow. The radiation model was based on the WSGG developed in Ref. [243]. They found that only the Eulerian-Eurlerian approach is able to capture the experimental trends. In addition, their simulations showed that RHT is the dominant mode of heat transfer in these flames and radiation from the participating gases contributes for 75% of the total RHT. Huyun et al. [245] modelled a 250 kW pilot scale combustion test facility (CTF) by using FLUENT. Simulations considered, on the one hand, a reference radiative model involving the non-grey WSGG coupled to Planck-mean radiative properties for the particles derived from Mie theory and, on the other hand, simplified radiative models based on grey formulations of the WSGG and simple constant or linear radiative properties for the particles. They found that the Mie theory improves considerably the prediction of the incident wall heat flux compared to the constant or linear models. Also the reference model was found to considerably improve the NOx prediction in the flame region. Guo et al. [246] carried out RANS simulations of the IFRF (International Flame Researcher Foundation) 250MW swirling oxy-coal flame using an Eulerian-Lagrangian description of flow and a gas-phase global mechanism coupled to the Eddy Dissipation Concept. The radiation model was based on the DOM coupled with the full spectrum k-distribution based weighted

sum-of-grey-gases model developed in Ref. [107]. Model predictions were found to agree well with the measurements. They showed that particle radiation influences significantly the flame temperature whereas the effects of burnout rate on particle radiative property are important to predict accurately the particle absorption after burnout.

8. Conclusions and perspectives

The present article reviewed the importance of RHT in combustion and the state-of-the-art radiation models for combustion applications. Special attention was paid to the RTE solvers and to the radiative properties of combustion gases and particles encountered in flames and combustion problems. As the focus is the applications of RHT models to turbulent flames and combustion systems, the state-of-the-art modeling of Turbulence-Radiation Interaction in both RANS and LES was also described. The following conclusions and recommendations can be drawn:

- Nowadays DOM and FVM are widely used as the RTE solver mainly due to their ease of implementation, fairly good accuracy, and often acceptable computational efficiency. According to some leaders in the RHT community, the Monte Carlo method could become the best choice in the future as computational power increases, at least for academic simulations. This assertion is confirmed by the recent increase in the number of simulations of flames and combustion systems involving Monte Carlo techniques, as reviewed in Section 7. Nevertheless, the computational cost related to RTE solvers remains a barrier to the application of non-grey radiation models in combustion problems and the development of new RTE solvers and the improvement of the computational efficiency of the existing ones should remain an active area of research.

- The modeling of non-grey gas RHT has benefited from the significant developments of FSCK/SLW models over the last two decades. These methods are sufficiently mature to be implemented in CFD codes for combustion simulations. They were proved to be accurate and can be applied to mixtures of gases and non-grey absorbing grey-scattering particles. In addition, the development of look-up tables has significantly improved their computational efficiency. Among these methods, the RC-FSK/RC-SLW model is recommended, since recent works suggested that it may be more accurate than the other schemes and it does not depend on the specification of a reference state. A remaining limitation is the application of SLW/FSCK to non-grey walls and/or non-grey scattering particles, which remains a challenge in RHT modeling.

- In the framework of RANS simulations, it was found that absorption TRI can be neglected in most situations by using the OTFA. On the other hand, emission TRI can be modelled accurately by using PDF approaches. For sooting turbulent flames, only transported PDF approaches that model the gas-soot turbulent couplings were found to be able to capture the negative correlation between soot volume fraction and temperature. This latter was found to play a fundamental role on soot emission. In LES, there is a consensus to neglect subgrid-scale absorption TRI whereas controversial conclusions were reached concerning the importance of subgrid-scale emission TRI. This term should depend on the configuration and a significant amount of work will be required to provide a full understanding and modeling recommendations.

The following other perspectives and remaining issues can be mentioned, although this list is far from being exhaustive:

- The availability of accurate spectroscopic and/or narrow band databases is a prerequisite for accurate modeling of gas radiative properties. Such databases are available for CO_2, H_2O, CO and CH_4. Because combustion systems at high pressure are of increasing interest, some questions remain about how to model the line wings at elevated pressure. In addition, no accurate data are available for most of the other gaseous hydrocarbon fuels, including evaporated liquid or solid fuels, such as n-heptane or PMMA. The knowledge of these data is fundamental to predict some phenomena such as the radiative feedback toward the liquid or solid fuel surfaces that drives the behaviour of fires. The radiative blockage due to the high concentrations of unburnt hydrocarbon fuels close to these surfaces is significant and becomes increasingly important with the size of the pool fire. On the other hand,.

- The spectrally-resolved thermal emissions from flames have been utilized for measurements of temperature, soot volume fraction, and certain gaseous species. Recently, flame synthesis of functional nanomaterials, such as nanotubes, nanowires, and metal-oxide nanoparticles, have received considerable attention for energy and sensor applications. The properties of these nanomaterials are strongly dependent on their size. Spectrally-resolved thermal emissions coupled with laser scattering measurements in the visible spectrum are attractive to offer a real-time online approach to monitor the synthesis conditions for obtaining the desired nanomaterials. Although in such applications the reverse Monte Carlo method is preferred, the challenge lies in how to efficiently deal with the effects of radiation scattering and also the co-existence of different scattering particles. Research is required to develop radiative transfer based diagnostics for online monitoring of nanomaterial synthesis in flames.

- Another emerging area in combustion application is the co-firing of gaseous hydrocarbon and micro-sized metal particles to reduce CO_2 emissions and at the same time to utilize waste metal materials. Similar to coal-fired combustion, radiation scattering by metal particles plays an important role in RHT and should be taken into account. The challenges in modeling RHT in such applications is that metal particles undergo phase change and therefore variations in their radiative properties. Research is needed to develop radiative property models to deal with the strong temperature dependence of metal particle radiative properties.

- Finally, there has been growing interest in combustion and heat transfer under supercritical conditions. To date, however, there appears to be no research conducted on the radiative properties of supercritical fluids. Available numerical studies of RHT at supercritical conditions assumed without justification that supercritical CO_2 and H_2O have the same radiative properties as their gaseous counterpart. Research of the radiative properties of supercritical fluids needs to be conducted to support RHT modeling in supercritical combustion and heat transfer applications.

Acknowledgements
PJC acknowledges the financial support of FCT-Fundação para a Ciência e Tecnologia, through IDMEC, under LAETA, project UID/EMS/50022/2019.

References

[1]. Hottel HC, Sarofim AF. Radiative Transfer. McGraw-Hill, New York, 1967.

[2]. Veynante D, Vervisch L. Turbulent combustion modeling. Prog. Ener. Combust. Sci. 2002; 28: 193: 26.
[3]. Echekki T, Mastorakos E. Turbulent Combustion Modeling. Advances, New Trends and Perspectives. Springer Verlag, Dordrecht, New York, 2011.
[4]. Coelho PJ. Numerical simulation of the interaction between turbulence and radiation in reactive flows, Prog. Ener. Combust. Sci. 2007; 33 : 311-383.
[5]. Modest MF, Haworth DC. Radiative Heat Transfer in Turbulent Combustion Systems: Theory and Applications. Springer: New-York; 2016.
[6]. Modest MF. Radiative Heat Transfer. 3nd ed. New York: Academic Press. 2013.
[7]. Bishop SR., Drysdale D.D. Fires in compartments: the phenomenon of flashover. Phil. Trans. R. Soc. Lond. A 1998; 356: 2855-2872.
[8]. Finney MA, Cohen JD, McAllister SS, Jolly WM. On the need for a theory of wildland fire spread. Int. J. Wildland Fire 2013; 22: 25-36.
[9]. Finney MA, Cohen JD, Forthofer JM, McAllister SS, Gollner MJ, Gorham DJ, Saito K, Akafuah NK, Adam BA, English JD. Role of buoyant flame dynamics in wildfire spread. PNAS. 2015; 112(32): 9833-9838.
[10]. Bedir H, T'ien JS. A computational study of flame radiation in PMMA diffusion flames including fuel vapor participation. Proc. Combust. Inst. 1998; 27: 2821-2828.
[11]. Demarco R, Nmira F, Consalvi JL. Influence of thermal radiation on soot production in Laminar axisymmetric diffusion flames. J. Quant. Spectrosc. Rad. Transf. 2013; 120: 52–69.
[12]. Guibaud A, Consalvi JL, Orlac'h JM, Citerne JM, Legros G. soot Production and Radiative Heat Transfer in Opposed Flame Spread over a Polyethylene Insulated Wire in Microgravity. Fire Technol. 2020; 56: 287-314.
[13]. Liu F, Guo H, Smallwood GJ, Gülder OL. Numerical modelling of soot formation and oxidationin laminar coflow non-smoking and smoking ethylene diffusion flames. Combust. Theor. Modelling 2003; 7: 301–315.
[14]. Cai J, Lei S, Dasgupta A, Modest MF, Haworth DC. High fidelity radiative heat transfer models for high-pressure laminar hydrogen–air diffusion flames. Combust Theor Model 2014; 18: 606–27.
[15]. Contreras J, Consalvi JL, Fuentes A. Numerical simulations of microgravity ethylene/air laminar boundary layer diffusion flames. Combust. Flame 2018; 191: 99-108.
[16]. Barlow RS, Carter CD. Raman/Rayleigh/LIF measurements of nitric oxide formation in turbulent hydrogen jet flames. Combust Flame 1994; 97: 261–80.
[17]. Nmira F, Consalvi JL, André F. Pressure effects on radiative heat transfer in hydrogen/air turbulent diffusion flames. J. Quant. Spectrosc. Rad. Transf. 2018; 220: 172-179.
[18]. Wang L, Modest MF, Haworth DC, Turns SR. Modelling nongrey gas-phase and soot radiation in luminous turbulent nonpremixed jet flames. Combust. Theor. Model. 2005; 9: 479-498.
[19]. Wang L, Endrud NE, Turns SR, D'Agostini MD, Slavejkov, AG. A study of the influence of oxygen index on soot, radiation, and emission characteristics of turbulent jet flames. Combust. Sci. Technol. 2002; 174: 45–72.
[20]. Viskanta R, Mengüç MP. Radiation heat transfer in combustion systems. Prog. Ener. Combust. Sci. 1987; 13:97-160.
[21]. Howell JR. Application of Monte Carlo to heat transfer problems. In: *Advances in Heat Transfer*, vol 5, ed. J P Hartnett and T Irvine, San Diego: Academic Press, pp 1–54, 1968.
[22]. Davison B. Neutron Transport Theory, London: Oxford University Press, 1958.

[23]. Carlson BG and Lathrop KD. Transport theory — The method of discrete ordinates. In: *Computing Methods in Reactor Physics*, ed. H Greenspan *et al*., New York: Gordon & Breach, 1968.
[24]. Fiveland WA. Discrete-ordinates solution of the radiative transport equation for rectangular enclosures. J. Heat Transfer 1984; 106: 699-706.
[25]. Raithby GD, Chui EH. A finite-volume method for predicting a radiant heat transfer in enclosures with participating media. J. Heat Transfer 1990; 112: 415-423.
[26]. Chai JC, Lee HS, Patankar SV. Finite volume method for radiation heat transfer. J Thermophys Heat Transf. 1990; 8: 419-425.
[27]. Wong BT, Mengüç MP. Comparison of Monte Carlo techniques to predict the propagation of a collimated beam in participating media. Numeric. Heat Transf. 2002; 42: 119-140.
[28]. Walters DV, Buckius RO. Rigorous development for radiation heat transfer in nonhomogeneous absorbing, emitting and scattering media. Int. J. Heat Mass Transf., 1992; 35: 3323-3333.
[29]. Case KM. Transfer problems and the reciprocity principle. Review Modern Physics. 1957; 29: 651-663.
[30]. Cherkaoui M, Dufresne JL, Fournier R, Grandpeix JY, Lahellec L. Monte Carlo simulation of radiation in gases with a narrow-band model and a net-exchange formulation. J. Heat Transf. 1996; 118: 401–407.
[31]. Cherkaoui M, Dufresne JL, Fournier R, Grandpeix JY, Lahellec L. Radiative net exchange formulation within one-dimensional gas enclosures with reflective surfaces. J. Heat Transf. 1998; 98: 275-278.
[32]. Tessé L, Dupoirieux F, Zamuner B, Taine J. Radiative transfer in real gases using reciprocal and forward Monte Carlo methods and a correlated-*k* approach. Int. J. Heat Mass Transf. 2002; 45: 2797-2814.
[33]. Wang A, Modest MF. Photon Monte Carlo simulation for radiative transfer in gaseous media represented by discrete particle fields. J. Heat Transf. 2006; 128: 1041-1049.
[34]. Pope SB. PDF methods for turbulent reactive flows. Prog. Energy Combust. Sci. 1985; 11: 119-192.
[35]. Zeeb CN, Dolaghan JS, Burns PJ. An efficient Monte Carlo particle tracing algorithm for large, arbitrary geometries. Numer. Heat Transf., Part B. 2001; 39: 325–344.
[36]. Mazumder S. Methods to Accelerate ray tracing in the Monte Carlo Method for Surface-To-Surface Radiation Transport. J. Heat Transf. 2006; 128: 945–952.
[37]. Perez P, Paulin M, El Hafi M. Application of a computer graphics technique for radiative transfer simulation in multidimensional combustion systems. In: *Radiative Transfer – V. Proc. Fifth Int. Symp. Radiative Transfer* ICHMT Digital Library, Begell House, 2007.
[38]. Kahhali N, Rivière P, Soufiani A. Study of an oct-tree based Monte Carlo algorithm for gas radiative transfer in complex geometries. In: *Computational Thermal Radiation in Participating Media – Proc Eurotherm Seminar 83 (Lisbon, Portugal, 15–17 August 2009).* Ed. P Coelho, D Lemonnier, P Lybaert and N Selçuk, Lisbon: IST Press, pp 153–162, 2009.
[39]. Soucasse L, Rivière P, Soufiani A. Monte Carlo methods for radiative transfer in quasi-isothermal participating media, J. Quant. Spectrosc. Rad. Transf. 2013; 128: 34-42.
[40]. Galtier M, Blanco S, Caliot C, Coustet C, Dauchet J, El Hafi M, Eymet V, Fournier R, Gautrais J, Khuong A, Piaud B, Terrée G. Integral formulation of null-collision Monte Carlo algorithms, J. Quant. Spectrosc. Rad. Transf. 2013; 125: 57–68.
[41]. Eymet V, Poitou D, Galtier M, El Hafi M, Terrée G, Fournier R. Null-collision meshless Monte-Carlo - Application to the validation of fast radiative transfer solvers embedded in combustion simulators. J. Quant. Spectrosc. Rad. Transf. 2013; 129: 145-137.

[42]. Galtier M, Roger M, André F, Delmas A. A symbolic approach for the identification of radiative properties. J. Quant. Spectrosc. Rad. Transf. 2017; 196: 130–141.
[43]. Palluotto L, Dumont N, Rodrigues P, Gicquel O, Vicquelin R. Assessment of randomized Quasi-Monte Carlo method efficiency in radiative heat transfer simulations. J. Quant. Spectrosc. Rad. Transf. 2019; 236: 106570.
[44]. Farmer J, Roy S. A quasi-Monte Carlo solver for thermal radiation in participating media, J. Quant. Spectrosc. Rad. Transf. 2020; 242: 106753.
[45]. Gerardin J, Seiler N, Ruyer P, Trovalet L, Boulet P. P1 approximation, MDA and IDA for the simulation of radiative transfer in a 3D geometry for an absorbing scattering medium. J. Quant. Spectrosc. Rad. Transf. 2012; 113: 140–149.
[46]. Yang J, Modest MF. Elliptic PDE formulation of general, three-dimensional high-order PN-approximations for radiative transfer. J. Quant. Spectrosc. Rad. Transf. 2007; 104: 217-227.
[47]. Modest MF, Yang J. Elliptic PDE formulation and boundary conditions of the spherical harmonics method of arbitrary order for general three-dimensional geometries, J. Quant. Spectrosc. Rad. Transf. 2008; 109: 1641–1666.
[48]. Modest MF. Further development of the elliptic PDE formulation of the P_N approximation and its Marshak boundary conditions. Numeric. Heat Transf. Part B, 2012; 62 :181–202.
[49]. Ge W, Marquez R, Modest MF, Roy SP. Implementation of high-order spherical harmonics methods for radiative heat transfer on OPENFOAM. J. Heat Transf. 2015; 137: 052701.
[50]. Ge W, Modest MF, Marquez R. Two-dimensional axisymmetric formulation of high order spherical harmonics methods for radiative heat transfer. J. Quant. Spectrosc. Rad. Transf. 2015; 156: 58–66.
[51]. Ge W, Modest MF, Roy SP. Development of high-order PN models for radiative heat transfer in special geometries and boundary conditions. J. Quant. Spectrosc. Rad. Transf. 2016; 172: 98–109.
[52]. Coelho PJ. Mathematical formulation. Thermopedia, A-to-Z Guide to Thermodynamics, Heat & Mass Transfer, and Fluids Engineering. http://www.thermopedia.com/pt/content/9170/
[53]. Coelho PJ. A comparison of spatial discretization schemes for differential solution methods of the radiative transfer equation. J. Quant. Spectrosc. Rad. Transf. 2008; 109(2):189 – 200.
[54]. Koch R, Becker R. Evaluation of quadrature schemes for the discrete ordinates method. J. Quant. Spectrosc. Rad. Transf. 2004; 84: 423–435.
[55]. Ramankutty MA, Crosbie AL. Modified discrete-ordinates solution of radiative transfer in three-dimensional rectangular enclosures. J. Quant. Spectrosc. Rad. Transf. 1998; 60: 103–134.
[56]. Raithby GD. Evaluation of discretization errors in finite-volume radiant heat transfer predictions. Numerical Heat Transfer. Part B: Fundamentals, 1999; 36: 241–264.
[57]. Coelho PJ. Advances in the discrete ordinates and finite volume methods for the solution of radiative heat transfer problems in participating media. J. Quant. Spectrosc. Rad. Transf. 2014; 145: 121-146.
[58]. Hunter B, Guo Z. Conservation of asymmetry factor in phase function discretization for radiative transfer analysis in anisotropic scattering media. Int. J. Heat Mass Transf. 2012; 55: 1544–1552.
[59]. Granate P, Coelho PJ, Roger M. Radiative heat transfer in strongly forward scattering media using the discrete ordinates method. J. Quant. Spectrosc. Rad. Transf. 2016; 172; 100-120.
[60]. Tencer R. Ray effect mitigation through reference frame rotation. J. Heat Transf. 2016; 138: 112701

[61]. Soucasse L, Dargaville S, Buchan AG, Pain CC. A goal-based angular adaptivity method for thermal radiation modelling in non grey media. J. Quant. Spectrosc. Rad. Transf. 2017; 200: 215–224.
[62]. Zhang B, Zhang L, Liu C, Chen Y. Goal-oriented regional angular adaptive algorithm for the S_N equations. Nuclear Sci. Eng. 2018; 189:·120–134.
[63]. Cai J, Roy S, Modest MF. A comparison of specularly reflective boundary conditions and rotationally invariant formulations for discrete ordinate methods in axisymmetric geometries. J. Quant. Spectrosc. Rad. Transf. 2016; 182: 75–86.
[64]. Le Hardy D, Favennec,Y, Rousseau B, Hecht F. Specular reflection treatment for the 3D radiative transfer equation solved with the discrete ordinates method. J. Comp. Phys. 2017; 334: 541–572.
[65]. Sun Y, Zhang X, Howell JR. Assessment of different radiative transfer equation solvers for combined natural convection and radiation heat transfer problems. J Quant Spectrosc Radiat Transf 2017;194:31–46.
[66]. Modest MF, Cai J, Ge W, Lee E. Elliptic formulation of the simplified spherical harmonics method in radiative heat transfer. Int. J. Heat Mass Transf 2014;76:459–466.
[67]. Pal G, Gupta A, Modest MF, Haworth DC. Comparison of accuracy and computational expense of radiation models in simulation of non-premixed turbulent jet flames. Combust. Flame 2015; 162: 2487-2495.
[68]. Solovjov VP, Webb BW, André F. Radiative properties of gases, Handbook of Thermal Science and Engineering, ed. F. Kulacki, Springer, New York, vol. 2, pp. 1-74, 2018.
[69]. Pearson JT, Webb BW, Solovjov V, Ma J. Effect of total pressure on the absorption line blackbody distribution function and radiative transfer in H_2O, CO_2, and CO. *J. Quant. Spectr. Rad. Transfer* 2018; 143: 100-110.
[70]. Pearson JT, Webb BW, Solovjov VP, Ma J. Efficient representation of the absorption line blackbody distribution function for H_2O, CO_2 and CO at variable temperature, mole fraction, and total pressure. J. Quant. Spectrosc. Radiat. Transf. 2014; 138: 82-96.
[71]. Pearson JT, Webb BW, Solovjov VP, Ma J. The absorption line blackbody distribution function and radiative transfer in H_2O, CO_2 and CO, J. Quant. Spectrosc. Radiat. Transf. 2014; 143: 100-110.
[72]. Chu H, Gu M, Consalvi JL, Liu F, Zhou H. Effects of total pressure on non-grey gas radiation transfer in oxy-fuel combustion using the LBL, SNB, SNBCK, WSGG, and FSCK methods. J. Quant. Spectrosc. Radiat. Transf. 2016; 172: 24-35.
[73]. Chu H, Consalvi JL, Gu M, Liu F. Calculations of radiative heat transfer in an axisymmetric jet diffusion flame at elevated pressures using different gas radiation models. J. Quant. Spectrosc. Radiat. Transf. 2017; 197: 12-25.
[74]. Rothman LS, Gordon IE, Barber RJ, Dothe H, Gamache RR, Goldman A, Perevalov VI, Tashkun SA, Tennyson J. HITEMP, the high-temperature molecular spectroscopic database. J. Quant. Spectrosc. Radiat. Transf. 2010; 111: 2139-2150.
[75]. Rivière P, Soufiani A. Updated band model parameters for H_2O, CO_2,CH_4 and CO radiationat high temperature. Int. J. Heat Mass Transf. 2012; 55: 3349-3358.
[76]. Kez V, Consalvi JL, Liu F, Ströhle J, Epple B. Assessment of several gas radiation models for radiative heat transfer calculations in a three-dimensional oxy-fuel furnace under coal-fired conditions. Int. J. Thermal Sci. 2017; 120: 289-302.
[77]. Consalvi JL, Nmira F. Simulations of sooting turbulent jet flames using a hybrid flamelet/stochastic Eulerian field method. Combust. Theory Model. 2016; 20: 221-257.
[78]. Dorigon LJ, Duciak G, Brittes R, Cassol F, Galarça M, França FHR. WSGG correlations based on HITEMP2010 for computation of thermal radiation in non-isothermal, non-homogeneous H_2O/CO_2 mixtures. Int. J. Heat Mass Transf. 2013; 64: 863-873.

[79]. Denison MK, Webb BW. A spectral line based weighted-sum-of-gray-gases model for arbitrary RTE solvers. J. Heat Transf. 1993; 115: 1004–1012.
[80]. Denison MK, Webb BW. The spectral-line-based weighted-sum-of-gray-gases model in nonisothermal nonhomogeneous media. J. Heat Transf. 1995; 117: 359–365
[81]. Denison MK, Webb BW. Development and application of an absorption line blackbody distribution function for CO2. Int. J. Heat Mass Transf. 1995; 38: 1813–1821.
[82]. Denison MK, Webb BW. The spectral-line weighted-sum-of-gray-gases model for H2O/CO2 mixtures. J. Heat Transf. 1995; 117: 788–792.
[83]. Pierrot L, Soufiani A, Taine J. Accuracy of narrow-band and global models for radiative transfer in H_2O, CO_2, and H_2O–CO_2 mixtures at high temperature. J. Quant. Spectrosc. Radiat. Transf. 1999; 62: 523–548.
[84]. Modest MF. Narrow-band and full-spectrum k-distributions for radiative heat transfer correlated-*k* vs. scaling approximation. J. Quant. Spectrosc. Radiat. Transf. 2003; 76(1): 69–83.
[85]. Kangwanpongpan T, França FHR, Corrêa da Silva R, Smith Schneider P, Krautz HJ. New correlations for the weighted-sum-of-gray-gases model in oxy-fuel conditions based on HITEMP 2010 database. Int. J. heat Mass Transf. 2012; 55: 7419–7433.
[86]. Bordbar MH, Węcel G, Hyppänen T. A line by line based weighted sum of gray gases model for inhomogeneous CO2–H2O mixture in oxy-fired combustion. Combust. Flame 2014; 161: 2435-2445.
[87]. Centeno PR, Brittes R, Rodrigues LGP,. Coelho FR, França FHR. Evaluation of the WSGG model against line-by-line calculation of thermal radiation in a non-gray sooting medium representing an axisymmetric laminar jet flame. Int. J. Heat Mass Transfer 2018; 124: 475–483.
[88]. Cassol F, Brittes R, França FHR, Ezekoye OA. Application of the weighted-sum-of-gray-gases model for media composed of arbitrary concentrations of H_2O, CO_2 and soot. Int. J. Heat Mass Transfer 2014; 79: 796–806.
[89]. Kez V, Liu F, Consalvi JL, Ströhle J, Epple B. A comprehensive evaluation of different radiation models in a gas turbine combustor under conditions of oxy-fuel combustion with dry recycle. J. Quant. Spectrosc. Radiat. Transf. 2016; 172: 121-133.
[90]. Clements AG, Porter R, Pranzitelli A, Pourkashaniana M. Evaluation of FSK models for radiative heat transfer under oxyfuel conditions. J. Quant. Spectrosc. Radiat. Transf. 2015; 151: 67-75.
[91]. Modest MF, Zhang H. The full spectrum correlated-*k* distribution for thermal radiation from molecular gas particulate mixtures. ASME J. Heat Transf. 2002; 124: 30-38, 2002.
[92]. Solovjov VP, Webb BW, André F. The rank correlated FSK model for prediction of gas radiation in non-uniform media, and its relationship to the rank correlated SLW model. *J. Quant. Spectr. Rad. Transfer*; 2018; 214: 130-132, 2018.
[93]. Webb BW, Solovjov VP, André F. The spectral line weighted-sum-of-gray-gases (SLW) model for prediction of radiative transfer in molecular gases, *Advances in Heat Transfer*, E.M. Sparrow, J.P. Abraham, J.M. Gorman, and W.J. Minkowycz, Eds., Academic Press, vol. 51, pp. 207-298, 2019.
[94]. André F, Solovjov VP, Lemonnier D, Webb BW. Co-monotonic global spectral models of gas radiation in nonuniform media based on arbitrary probability measures. J. Appl. Math. Modeling 2017; 50: 741-754.
[95]. Solovjov VP, André F, Lemonnier D, Webb BW. The generalized SLW model, Eurotherm105: Computational Thermal Radiation in Participating Media V, *J. Physics*: Conf. Series, 2016; 012022,676: 1-36.

[96]. Cai J, Modest MF. Improved full-spectrum *k*-distribution implementation for inhomogeneous media using a narrow-band database. *J*. Quant. Spectr. Rad. Transf. 2014; 141: 65-72.
[97]. Solovjov VP, André F, Lemonnier D, Webb BW. The rank correlated SLW model of gas radiation in non- uniform media. J. Quant. Spectr. Rad. Transf.2017; 197: 26-44.
[98]. Solovjov VP, Webb BW, André F, Lemonnier D. Locally correlated SLW model for prediction of gas radiation in non-uniform media and its relationship to other global methods, J. Quant. Spectr. Rad. Transfer 2020; 245: 106857.
[99]. André F, Coelho F, Consalvi JL, França F, Galtier M, Nmira F, Solovjov VP, Webb BW. Accuracy of engineering methods for radiative heat transfer in CO_2-H_2O mixtures at high temperature. RAD 19, Athens, Greece, 2019.
[100]. Wang C, Modest MF, He B. Improvement of full-spectrum k-distribution method using quadrature transformation. Int. J. Thermal Sci. 2016; 108: 100-107.
[101]. Wang C, Ge W, Modest MF, He B. A full-spectrum k-distribution look-up table for radiative transfer in nonhomogeneous gaseous media. J. Quant. Spectrosc. Radiat. Transf. 2016; 168: 46–56.
[102]. Wang C, Ge W, Modest MF, He B. Full-spectrum k-distribution look-up table for nonhomogeneous gas–soot mixtures. J. Quant. Spectrosc. Radiat. Transf. 2016; 176: 129-136.
[103]. Wang C, He B, Modest MF, Ren T. Efficient full-spectrum correlated- k -distribution look-up table. J. Quant. Spectrosc. Radiat. Transf. 2018; 219: 108-116.
[104]. Wang C, He B, Modest MF. Full-spectrum correlated-k-distribution look-up table for radiative transfer in nonhomogeneous participating media with gas-particle mixtures. Int. J. Heat Mass Transf. 2019; 137: 1053–1063.
[105]. Solovjov VP, Webb BW. An Efficient Method for Modeling Radiative Transfer in Multicomponent Gas Mixtures with Soot. ASME J. Heat Transf. 2001; 123: 450-457.
[106]. Kez V, Consalvi JL, Liu F, Gronarz T, Ströhle J, Kneer R, Epple B. Investigation of gas and particle radiation modelling in wet oxy-coal combustion atmospheres. Int. J. Heat Mass Transf. 2019; 133: 1026-1040.
[107]. Guo J, Hu F, Luo W, Li P, Liu Z. A full spectrum k-distribution based non-gray radiative property model for fly ash particles. Int. J. Heat Mass Transf. 2018; 118: 103-115.
[108]. Guo J, Hu F, Luo W, Li P, Liu Z. A full spectrum k -distribution based non-gray radiative property model for unburnt char. Proc. Combust. Inst. 2019; 37: 3081-3089.
[109]. Modest MF, Riazzi RJ. Assembly full spectrum k-distribution from a narrow band database: effects of mixing gases, gases and non-gray absorbing particles and non-gray scatters in non-gray enclosures, J. Quant. Spectrosc. Radiat. Transf. 2005, 90: 169-189.
[110]. Olfert J, Rogak S. Universal relationships between soot effective density and primary particle size for common combustion sources, Aerosol Sci. Technol. 2019; 53: 485-492.
[111]. Sorensen CM. Light scattering by fractal aggregates: a review. Aerosol Science and Technology 2001; 35: 648-687.
[112]. Eymet V, Brasil AM, El Hafi M, Farias TL, Coelho PJ. Numerical investigation of the effect of soot aggregation on the radiative properties in the infrared region and radiative heat transfer, J. Quant. Spectrosc. Radiat. Transf. 2002; 74: 697-718.
[113]. Michelsen, H.A. Probing soot formation, chemical and physical evolution, and oxidation: a review of in situ diagnostic techniques and needs. Proc. Combust. Inst. 2017; 36(1): 717-735.
[114]. Yon J, Bescond A, Liu F. On the radiative properties of soot aggregates part 1: necking and overlapping. J. Quant. Spectrosc. Radiat. Transf. 2015; 162: 197-206.

[115]. Liu F, Yon J, Fuentes A, Lobo P, Smallwood GJ, Corbin JC. Review of recent literature on the light absorption properties of black carbon: refractive index, mass absorption cross section, and absorption function. Aerosol Sci. Technol. 2019; 54: 33-51.
[116]. Chang H, Charalampopoulos TT. Determination of the wavelength dependence of refractive indices of flame soot. Proc. Roy. Soc. Lond. A 1990; 430: 577-591.
[117]. Solovjov VP, Webb BW. An efficient method for modeling of radiative transfer in multicomponent gas mixtures with soot particles ASME J. Heat Transf. 2011; 123: 450-457.
[118]. Wang H. Formation of nascent soot and other condensed-phase materials in flames. Proc. Combust. Inst. 2011; 33: 41-67.
[119]. Eberle C, Gerlinger P, Aigner M. A sectional PAH model with reversible PAH chemistry for CFD soot simulations. Combust. Flame 2017; 179: 63-73.
[120]. Bohren CF, Huffman DR. Absorption and Scattering of Light by Small Particles, John Wiley & Sons, New York, 1983.
[121]. Manickavasagam M. Mengüç MP. Effective optical properties of pulverized coal particles determined from FT-IR spectrometer experiments. Ener. Fuels 1993 7: 860-869.
[122]. Yang X, Clements A, Szuhánszki J, Huang X, Moguel OF, Li J, Gibbins J, Liu Z, Zheng C, Ingham D, Ma L, Nimmo B, Pourkashanian M. Prediction of the radiative heat transfer in small and large scale oxy-coal furnaces, Appl. Ener. 2018; 211: 523-537.
[123]. Schiemann M, Gronarz T, Graeser P, Gorewoda J, Kneer R, Scherer V. A correlation between char emissivity and temperature. Fuel 2019; 256: 115889.
[124]. Goodwin D, Mitchner M, Fly-ash radiative properties and effect on radiative heat transfer in coal-fired systems. Int. J. Heat Mass Transfer 1989; 32:627-638.
[125]. Ateş C, Selçuk N, Kulah G. Influence of fly ash composition on non-gray particle radiation in combustion systems. J. Quant. Spectrosc. Radiat. Transf. 2018; 215: 25-40.
[126]. Dombrovsky LA, Baillis D. Thermal Radiation in Disperse Systems: An Engineering Approach. Begell House, New York, 2010.
[127]. Fisher SJ, Hardouin-Duparc B, Grosshandler WL. The structure and radiation of an ethanol pool fire. Combust. Flame 1987 ; 70 : 291-306.
[128]. Jeng SM, M.C. Lai, G.M. Faeth. Nonluminous radiation in turbulent buoyant axsymmetric flames, Combust. Sci Technol. 1984 : 40 ; 41-53.
[129]. Jeng SM, Faeth GM. Radiative heat fluxes near turbulent buoyant methane diffusion flames. J. Heat Transf. 1984 ; 106 : 886-888.
[130]. Gore JP, Faeth GM. Structure and spectral radiation properties of turbulent ethylene/air diffusion flames. Proc. Combust. Inst. 1986 ; 21 : 1521-1531.
[131]. Gore JP, Jeng SM, Faeth GM. Spectral and total radiation properties of turbulent carbon monoxide/air diffusion flames. AIAA J 1987 ; 25 : 339-345.
[132]. Gore JP, Faeth GM. Structure and radiation properties of luminous turbulent acetylene/air diffusion flames. J. Heat Transf. 1988 ; 110 : 173-181.
[133]. Kounalakis ME, Gore JP, Faeth GM. Turbulence/radiation interactions in nonpremixed hydrogen/air flames. Proc. Combust. Inst. 1988 ; 22 : 1281-1290.
[134]. Kounalakis ME, Gore JP, Faeth GM. Mean and fluctuating radiation properties of nonpremixed turbulent carbon monoxide/air flames. J. Heat Transf. 1989 ; 111 : 1021-1030.
[135]. Kounalakis ME, Sivathanu YR, Faeth GM. Infrared radiation statistics of nonluminous turbulent diffusion flames. J. Heat Tansf. 1991 ; 113 : 437-445.
[136]. Mazumder S, Modest M.F. A probability density function approach to modeling turbulence-radiation interactions in nonluminous flames. Int. J. Heat Mass Transf. 1999; 42 : 971-991.

[137]. Li G, Modest MF. Application of composition pdf method in the investigation of turbulence-radiation interactions. J. Quant. Spectrosc. Radiat. Trans. 2002; 73: 461-472.
[138]. Li G, Modest MF. Importance of turbulence-radiation interactions in turbulent reacting flows. J. Heat Trans. 2003; 125 : 454-462.
[139]. Coelho PJ, Teerling OJ, Roekaerts D. Spectral radiative effects and turbulence/radiation interaction in a non-luminous turbulent diffusion jet flame. Combust. Flame 2003 ; 133 : 75-91.
[140]. Tessé L, Dupoirieux F, Taine J. Monte Carlo Modeling of radiative transfer in a turbulent sooty flame. Int. J. Heat Mass Transf. 2004 ; 47 : 555-572.
[141]. Coelho PJ. Detailed numerical simulation of radiative transfer in nonluminous turbulent jet diffusion flame. Combust. Flame 2004; 136: 481-492.
[142]. Habibi A, Merci B, Roekaerts D. Turbulence radiation interaction in Reynold-averaged Navier-Stokes simulations of nonpremixed piloted turbulent laboratory scale flames, Combust. Flame 2007; 151: 303-320.
[143]. Mehta RS, Modest MF, Haworth DC. Radiation characteristics and turbulence–radiation interactions in sooting turbulent jet flames, Combust. Theory Model. 2010 ; 14 : 105-124.
[144]. Consalvi JL. Influence of turbulence–radiation interactions in laboratory-scale methane pool fires. Int. J. Thermal Sci. 2012; 60: 122-130.
[145]. Coelho PJ. A theoretical analysis of the influence of turbulence on radiative emission in turbulent diffusion flames of methane. Combust. Flame 2013; 160 : 610-617.
[146]. Nmira F, Consalvi JL, André F. Pressure effects on radiative heat transfer in hydrogen/air turbulent diffusion flames. J. Quant. Spectros. Rad. Transf. 2018; 220: 172-179.
[147]. Fraga GC, Centeno FR, Petry AP, Coelho PJ, França FHR. On the individual importance of temperature and concentration fluctuations in the turbulence-radiation interaction in pool fires. Int. J. Heat and Mass Transf. 2019; 136: 1079–1089.
[148]. Yang X, He Z, Niu Q, Dong S, Tan H. Numerical analysis of turbulence radiation interaction effect on radiative heat transfer in a swirling oxyfuel furnace. Int. J. Heat Mass Transf. 2019; 14 : 1227–1237.
[149]. Nmira F, Liu Y, Consalvi, Andre F, Liu F. Pressure Effects on Radiative Heat Transfer in Sooting Turbulent Diffusion Flames. J. Quant. Spectros. Rad. Transf. 2020; doi.org/10.1016/j.jqsrt.2020.106906.
[150]. Wang A, Modest MF, Haworth DC, Wang L. Monte Carlo simulation of radiative heat transfer and turbulence interactions in methane/air jet flames. J. Quant. Spectros. Rad. Transf. 2008; 109: 269-279.
[151]. Rodrigues P, Gicquel O, Franzelli B, Darabiha N, Vicquelin R. Analysis of radiative transfer in a turbulent sooting jet flame using a Monte Carlo method coupled to large eddy simulation. J. Quant. Spectros. Rad. Transf. 2019; 235: 187–203.
[152]. Consalvi JL, Nmira F. Effects of soot absorption coefficient–Planck function correlation on radiative heat transfer in oxygen-enriched propane turbulent diffusion flame, J. Quant. Spectros. Rad. Transf. 2016; 172: 50-57.
[153]. Coelho PJ. Turbulence–Radiation Interaction: from theory to application in numerical simulations. J. Heat Transf. 2012; 134: 031001.
[154]. Consalvi JL, Nmira F. Absorption Turbulence-Radiation Interactions in Sooting Turbulent Jet Flames, J. Quant. Spectros. Rad. Transf. 2017; 201: 1-9.
[155]. Kabashinikov VP, Myasnikova GI. Thermal radiation in turbulent flows-temperature and concentration fluctuations. Heat Transf.-Sov. Res. 1985; 17: 16-125.
[156]. Song TH, Viskanta R. Interaction of radiation with turbulence: application to a combustion system. J. Thermophys. Heat Transf. 1987; 1: 56-62.

[157]. Consalvi JL, Demarco R, Fuentes A, Melis S, Vantelon JP. On the modeling of radiative heat transfer in pool fires. Fire Safety J. 2013; 60: 73-81.
[158]. Lee SY, Turns SR, Santoro RJ. Measurements of soot, OH, and PAH concentrations in turbulent ethylene/air jet flames. Combust. Flame 2009; 156: 2264-2275.
[159]. Ren T, Modest MF, Haworth DC. Simulating turbulence–radiation interactions using a presumed probability density function method. Int. J. Heat and Mass Transf. 2018; 232: 911-923.
[160]. Snegirev YA. Statistical modeling of thermal radiation transfer in buoyant turbulent diffusion flames. Combust. Flame 2004; 136: 51-71.
[161]. Fraga GC, Coelho PJ, Petry AP, França FRH. Development and testing of a model for turbulence-radiation interaction effects on the radiative emission. J. Quant. Spectros. Rad. Transf. 245 (2020) doi.org/10.1016/j.jqsrt.2020.106852
[162]. Sivathanu YR, Gore JP, Dolinear J. Transient scalar properties of strongly radiating jet flames, Combust. Sci. and Tech. 1991; 76: 45-66.
[163]. Sivathanu YR, Gore JP. Transient structure and radiation properties of strongly radiating buoyant flames. J. Heat Transf. 1992; 114: 659-65.
[164]. Murphy JJ, Shaddix CR. Soot properties and species measurements in a two-meter diameter JP-8 pool fire. Sandia Report, SAND20034246, 2003.
[165]. Zeng D, Chatterjee P, Wang Y. The effect of oxygen depletion on soot and thermal radiation in buoyant turbulent diffusion flames, Proc. Combust. Inst. 2019; 37: 825-32.
[166]. Kollmann W, Kennedy IM, Metternich M, Chen JY. Application of a soot model to a turbulent ethylene diffusion flame. In: Bockhorn H, editors. Soot Formation in Combustion: Mechanism and Models, Berlin: Springer-Verlag, 1994.
[167]. Nmira F, Burot D, Consalvi JL. Soot emission radiation–turbulence interactions in diffusion jet flames. Combust. Sci. Technol. 2019; 191: 126-36.
[168]. Nmira F, Consalvi JL, Delichatsios MA. Radiant fraction from sooting jet fires. Combust. Flame 2019; 208: 51-62.
[169]. Coelho PJ. Approximate solutions of the filtered radiative transfer equation in large eddy simulations of turbulent reactive flows. Combust. Flame 2009; 156: 1099-1110.
[170]. Consalvi JL, Nmira F, Kong W. On the modeling of the filtered radiative transfer equation in large eddy simulations of lab-scale sooting turbulent diffusion flames. J. Quant. Spectrosc. Radiat. Transf. 2018; 221: 51–60.
[171]. Gupta A, Haworth DC, Modest MF. Turbulence-radiation interactions in large-eddy simulations of luminous and nonluminous nonpremixed flames. Proc. Combust. Inst. 2013; 34: 1281–1288.
[172]. Miranda FC, Coelho P, di Mare F, Janicka J. Study of turbulence-radiation interactions in large-eddy simulation of scaled Sandia flame D. J. Quant. Spectrosc. Radiat. Transf. 2019; 228: 47–56.
[173]. Miranda FC, Coelho P, Strölhe, Janicka J. Large-eddy simulation of a bluff-body stabilised nonpremixed flame with radiation heat transfer. Combust. Theory and Modelling 2020; doi.org/10.1080/13647830.2020.1727017.
[174]. Chatterjee P, Wang Y, Meredith KV, Dorofeev SB. Application of a subgrid soot-radiation model in the numerical simulation of a heptane pool fire, Proc. Combust. Inst. 2015; 35: 2573–2580.
[175]. Sikic I, Dembele S, Wen J. Non-grey radiative heat transfer modelling in LES-CFD simulated methanol pool fires, J. Quant. Spectrosc. Radiat. Transf. 2019; 234: 78–89.
[176]. Snegirev A, Markus E, Kuznetsov E, Harris J, Wu T. On soot and radiation modeling in buoyant turbulent diffusion flames. Heat Mass Transf. 2018; 54: 2275–2293.
[177]. Spalding D.B. A theory of inflammability limits and flame-quenching. Proc. Roy. Soc. London A 1957; 240 (1220): 84-100.

[178]. Berlad, AL, Yang CH. A theory of flame extinction limits. Combust. Flame 1960; 4: 325-333.
[179]. Gerstein M, Stine WB. Analytical criteria for flammability limits. Proc. Combust. Inst. 1973; 14: 1109-1118.
[180]. Ronney PD. Effect of Chemistry and Transport Properties on Near-Limit Flames at Microgravity. Combust. Sci. Technol. 1988; 59: 123-141.
[181]. Lakshmisha KN, Paul PJ, Mukunda HS. On the flammability limit and heat loss in flames with detailed chemistry. Proc. Combust. Inst. 1991; 23: 433-440.
[182]. Ju Y, Guo H, Maruta K, Liu F. On the extinction limit and flammability limit of non-adiabatic stretched methane-air premixed flames. J. Fluid Mech. 1997; 342: 315-334.
[183]. Ju Y, Masuya G, Ronney PD. Effects of radiative emission and absorption on the propagation and extinction of premixed gas flames. Proc. Combust. Inst. 1998; 27: 2619-2626.
[184]. Hubbard GL, Tien CL. Infrared Mean Absorption Coefficients of Luminous Flames and Smoke. J. Heat Transf. 1978; 100(2): 235-239.
[185]. Williams FA. Combustion theory. Addison-Wesley, Reading, Massachusetts,1985.
[186]. Joulin G, Eulier M. Radiation-dominated propagation and extinction of slow, particle-laden gaseous flames. Proc. Combust. Inst. 1989; 22: 1579-1585.
[187]. Chen Z, Qin X, Xu B, Ju Y, Liu F, Studies of radiation absorption on flame speed and flammability limit of CO2 diluted methane flames at elevated pressures, Proc. Combust. Inst. 2007; 31: 2693-2700.
[188]. Maruta K, Yoshida M, Ju Y, Niioka T. Experimental study on methane-air premixed flame extinction at small stretch rates in microgravity. Proc. Combust. Inst. 1996; 26: 1283-1289.
[189]. Guo H, Ju Y, Maruta K, Niioka T, Liu F. Radiation extinction limit of counterflow premixed lean methane-air flames. Combust. Flame (1997) 109:639-646.
[190]. Tien CL. Thermal radiation properties of gases, Advances in Heat Transfer. 1969; 5: 253-324.
[191]. Ju Y, Guo H, Liu F, Maruta K. Effects of the Lewis number and radiative heat loss on the bifurcation and extinction of CH_4/O_2-N_2-He flames. J. Fluid Mech. 1999; 379: 165-190.
[192]. Soufiani A, Taine J. High temperature gas radiative property parameters of statistical narrow-band model for H_2O, CO_2 and CO, and correlated-K model for H_2O and CO_2, Int. J. Heat Mass Transfer 1997; 40(4): 987-991.
[193]. Guo H, Ju Y, Maruta K, Liu F. Numerical investigation of CH_4/CO_2/air and $CH_4/CO_2/O_2$ counterflow premixed flames with radiation reabsorption. Combust. Sci. Technol. 1998; 135: 49-64.
[194]. Ju Y, Law CK, Maruta K, Niioka T. Radiation-induced instability of stretched premixed flames, Proc. Combust. Inst. 2000; 28: 1891-1900.
[195]. Liñán A. The asymptotic structure of counterflow diffusion flames for large activation energies. Acta Astronaut. 1974; 1: 1007–1039.
[196]. T'ien JS, Foutch DW. Extinction of a stagnation-point diffusion flame at reduced gravity. AIAA J. 1987; 25: 972–976.
[197]. Bonne U. Radiative extinguishment of diffusion flames at zero gravity. Combust. Flame 1971; 16 : 147-159.
[198]. T'ien JS. Diffusion flame extinction at small stretch rates: the mechanism of radiative loss. Combust. Flame 1986; 65: 31-34.

[199]. Platt JA, T'ien JS. Chemical and physical processes in combustion. Fall Technical Meeting, Easten Section of the Combustion Institute, 1990.
[200]. Liu Y, Rogg B. Modelling of thermally radiating diffusion flames with detailed chemistry and transport. In Heat Transfer in Radiating and Combustion Systems (ed. M.G. Carvalho, F. Lockwood, and J. Taine), pp. 114–127, 1991, Springer.
[201]. Maruta K, Yoshida M, Guo H, Ju Y, Niioka T. Extinction of low-stretched diffusion flame in microgravity. Combust. Flame 1998; 112: 181-187.
[202]. Mills K, Matalon M. Extinction of spherical diffusion flames in the presence of radiant loss. Proc. Combust. Inst. 1998; 27: 2535–2541.
[203]. Wang Q, Chao BH. Kinetic and radiative extinctions of spherical burner-stabilized diffusion flames. Combust. Flame 2011; 158: 1532–1541.
[204]. Tse SD, Zhu D, Sung CJ, Ju Y, Law CK. Microgravity burner-generated spherical diffusion flames: experiment and computation. Combust. Flame 2001; 125: 1265–1278.
[205]. Santa K, Chao B, Sunderland PB, Urban D, Stocker D, Axelbaum R. Radiative extinction of gaseous spherical diffusion flames in microgravity. Combust. Flame 2007; 151: 665–675.
[206]. Santa KJ, Sun Z, Chao BH, Sunderland PB, Axelbaum RL, Urban DL, Stocker DP. Numerical and experimental observations of spherical diffusion flames. Combust. Theory Model. 2007; 11: 639–652.
[207]. Chernovsky MK, Atreya A, Im HG. Effect of CO_2 diluent on fuel versus oxidizer side of spherical diffusion flames in microgravity. Proc. Combust. Inst. 2007; 31: 1005–1013.
[208]. Tang S, Chernovsky MK, Im HG, Atreya A. A computational study of spherical diffusion flames in microgravity with gas radiation. Part I: model development and validation. Combust. Flame 2010; 157 : 118–126.
[209]. Tang S, Im HG, Atreya A. A computational study of spherical diffusion flames in microgravity with gas radiation. Part II: parametric studies of the diluent effects on flame extinction. Combust. Flame 2010; 157, 127–136.
[210]. Rodenhurst III MK, Chao BH, Sunderland PB, Axelbaum RL. Structure and extinction of spherical burner-stabilized diffusion flames that are attached to the burner surface. Combust. Flame 2018; 187: 22–29
[211]. Fuentes A, Legros G, Claverie A, Joulain P, Vantelon JP, Torero JL. Interactions between soot and CH radicals in a laminar boundary layer type diffusion flame in microgravity. Proc. Combust. Inst. 2007; 31: 2685–2692.
[212]. Legros G, Fuentes A, Rouvreau S, Joulain P, Porterie B, Torero JL. Transport mechanisms controlling soot production inside a non-buoyant laminar diffusion flame. Proc. Combust. Inst. 2009; 32: 2461–2470.
[213]. Legros G, Torero JL. Phenomenological model of soot production inside a non-buoyant laminar diffusion flame. Proc. Combust. Inst. 2015; 35: 2545–2553.
[214]. Contreras J, Consalvi JL, Fuentes A. Oxygen index effect on the structure of a laminar boundary layer diffusion flame in a reduced gravity environment. Proc. Combust. Inst. 2017; 36: 3237-3245.
[215]. Bhattacharjee S, Altenkirch RA. Radiation-controlled, opposed-flow flame spread in a microgravity environment. Proc. Combust. Inst. 1991; 23: 1627–1633.
[216]. Liu F, Guo H, Smallwood GJ, Gülder ÖL. Effects of gas and soot radiation on soot formation in a coflow laminar ethylene diffusion flame. J. Quant. Spectrosc. Radiat. Heat Transf. 2002; 73: 409-421.

[217]. Liu F, Smallwood GJ, Kong W. The importance of thermal radiation transfer in laminar diffusionflames at normal and microgravity. J. Quant. Spectrosc. Radiat. Heat Transf. 2011; 112: 1241-1249.
[218]. Kong W, Liu F. Numerical study of the effects of gravity on soot formation in laminar coflow methane/air diffusion flames under different air stream velocities. Combust. Theor. Model. 2009; 13: 993-1023.
[219]. Guibaud A, Citerne J, Consalvi JL, Fujita O, Torero J, Legros G. Experimental evaluation of flame radiative feedback: methodology and application to opposed flame spread over coated wires in microgravity. Fire Technol. 2020; 56: 185–207.
[220]. Guibaud A, Citerne JM, Orlac'h JM, Fujita O, Consalvi JL, Torero JL, Legros G. Broadband modulated absorption/emission technique to probe sooting flames: Implementation, validation, and limitations. Proc. Combust. Inst. 2019; 37: 3959-3966.
[221]. Coelho PJ. Radiative Transfer in Combustion Systems. Handbook of Thermal Science and Engineering, ed. F. Kulacki, Springer, New York, 2017.
[222]. Zhang J, Shaddix CR, Schefer RW. Design of "model-friendly" turbulent non-premixed jet burners for C2+ hydrocarbon fuels. Review of Sci. Instrument 2011; 82: 074101.
[223]. Ihme M, Pitsch H. Modeling of radiation and nitric oxide formation in turbulent nonpremixed flames using a flamelet/progress variable formulation. Phys. Fluids 2008; 20: 1–20.
[224]. Mueller ME, Pitsch H. LES model for sooting turbulent nonpremixed flames. Combust Flame 2012; 159(6): 2166–80.
[225]. Wu B, Roy SP, Zhao X. Detailed modeling of a small-scale turbulent pool fire. Combust. Flame 2020; 214: 234-237.
[226]. Klassen M, Gore J. Structure and radiation properties of pool fires, NIST grant contract report. U.S. Department of Commerce. National Institute of Standards and Technology. 1992.
[227]. Consalvi JL, Nmira F. Transported scalar PDF modeling of oxygen-enriched turbulent jet diffusion flames: Soot production and radiative heat transfer. Fuel 2016; 178: 37-48.
[228]. Bolla M, Chishty MA, Hawkes E, Chan QN, Kook S. Influence of turbulent fluctuations on radiation heat transfer, NO and soot formation under ECN Spray A conditions. Proc. Combust. Inst. 2017; 36: 3551-3558.
[229]. Ferreyro Fernandez S, Paul C, Sircar A, Imren A, Haworth DC, Roy S, Modest MF. Soot and spectral radiation modeling for high-pressure turbulent spray flames. Combust. Flame 2018; 190: 402-415.
[230]. Mukut KM, Roy SP. Effect of O_2 concentration in ambient mixture and multiphase radiation on pollutant formation in ECN spray-A. Combust. Theor. Model. 2020. DOI: 10.1080/13647830.2020.1721561.
[231]. Roy SP, Cai J, Modest MF. Development of a multiphase photon Monte Carlo method for spray combustion and its application in high-pressure conditions. Int. J. Heat Mass Transf. 2017; 115 453–466.
[232]. Paul C, Ferreyro Fernandez S, Haworth DC, Roy S, Modest MF. A detailed modeling study of radiative heat transfer in a heavy-duty diesel engine. Combust. Flame 2019; 200: 325–341.
[233]. Paul C, Haworth DC, Modest MF. A simplified CFD model for spectral radiative heat transfer in high-pressure hydrocarbon–air combustion systems. Proc. Combustion Inst. 2019; 37: 4617–4624.
[234]. Berger S, Richard S, Duchaine F, Staffelbach G, Gicquel LYM. On the sensitivity

of a helicopter combustor wall temperature to convective and radiative thermal loads. Appl. Thermal Engineer. 2016; 103: 1450-1459.
[235]. Koren C, Vicquelin R, Gicquel O. Multiphysics simulation combining large-eddy simulation, wall heat conduction and radiative energy transfer to predict wall temperature induced by a confined premixed swirling flame. Flow, Turb. And Combust. 2018; 101: 72-102.
[236]. Poitou D, Amaya J, Bushan Singh C, Joseph D, Hafi M, Cuenot B. Validity limits for the global model FS-SNBCK for combustion applications. in: Eurotherm83 – Computational Thermal Radiation in Participating Media III, 2009.
[237]. Guiberti T, Durox D, Scoufaire P, Schuller T. Impact of heat loss and hydrogen enrichment on the shape of confined swirling flames. Proc. Combust. Inst. 2015; 35(2): 1385-1392.
[238]. Mercier R, Guiberti T, Chatelier A, Durox D, Gicquel O, Darabiha N, Schuller T, Fiorina B. Experimental and numerical investigation of the influence of thermal boundary conditions on premixed swirling flame stabilization. Combust. Flame 2016; 171: 42-58.
[239]. Koren C, Vicquelin R, Gicquel O. Self-adaptive coupling frequency for unsteady coupled,conjugate heat transfer simulations. Int. J. Thermal Sci. 2017; 38: 340-354.
[240]. Wu B, Roy SP, Zhao X, Modest MF. Effect of multiphase radiationon coal combustion in a pulverized coal jet flame. J. Quant. Spectrosc. Radiat. Transf. 2017 ; 197 : 154-165.
[241]. Zhang J, Ito T, Ito S, Riechelmann D, Fujimori T. Numerical investigation of oxy-coal combustion in a large-scale furnace: Non-gray effect of gas and role of particle radiation. Fuel 2015; 139: 83-97.
[242]. Adams BR, Hosler TR. Pressure and particle property impacts on radiation in oxy-coal combustion. Fuel 2019; 239: 667-76.
[243]. Seidel T, Krishnamoorthy G, Seames WS. Characterizing flame stability and radiative heat transfer in non-swirling oxy-coal flames using different multiphase modeling frameworks. Fuel 2019; 256: 115948.
[244]. Krishnamoorthy G. A new weighted-sum-of-gray-gases model for oxy-combustion scenarios. Int. J. Energy Res 2013; 37(14): 1752–63.
[245]. Huynh H, Clements AG, Szuhánszki J, Gale WF, Ma L, Ingham DB, M. Pourkashanian. Investigation of particle radiation and its effect on NO prediction in a pilot-scale facility for both air and oxy-coal combustion. Fuel 2019; 250: 254-64.
[246]. Guo J, Hu F, Jiang X, Li P, Liu Z. Effects of gas and particle radiation on IFRF 2.5 MW swirling flame under oxy-fuel combustion. Fuel 2020; 263: 116634.